



RESEARCH ARTICLE

10.1029/2023JD039002

Interannual Variability of Zonal Mean Temperature, Water Vapor, and Clouds in the Tropical Tropopause Layer

Aodhan Sweeney¹  and Qiang Fu¹

¹Department of Atmospheric Sciences, University of Washington, Seattle, WA, USA

Key Points:

- The interannual variability in the cold point tropopause temperature averaged over 15°S–15°N is driven by stratospheric processes
- This cold point tropopause temperature residual after regressing out large-scale modes is still correlated with stratospheric temperature
- The portion of the BDC's shallow branch, which is independent of our eddy heat flux BDC index, is an important source of TTL variability

Supporting Information:

Supporting Information may be found in the online version of this article.

Correspondence to:

A. Sweeney,
aodhan@uw.edu

Citation:

Sweeney, A., & Fu, Q. (2024). Interannual variability of zonal mean temperature, water vapor, and clouds in the tropical tropopause layer. *Journal of Geophysical Research: Atmospheres*, 129, e2023JD039002. <https://doi.org/10.1029/2023JD039002>

Received 4 APR 2023

Accepted 13 JAN 2024

Author Contributions:

Conceptualization: Qiang Fu
Data curation: Aodhan Sweeney
Formal analysis: Aodhan Sweeney
Funding acquisition: Aodhan Sweeney, Qiang Fu
Investigation: Aodhan Sweeney, Qiang Fu
Methodology: Aodhan Sweeney, Qiang Fu
Project Administration: Qiang Fu
Software: Aodhan Sweeney
Supervision: Qiang Fu
Visualization: Aodhan Sweeney
Writing – original draft: Aodhan Sweeney
Writing – review & editing: Qiang Fu

© 2024. The Authors.

This is an open access article under the terms of the [Creative Commons Attribution License](https://creativecommons.org/licenses/by/4.0/), which permits use, distribution and reproduction in any medium, provided the original work is properly cited.

Abstract Water vapor and cirrus clouds in the tropical tropopause layer (TTL) are important for the climate and are largely controlled by temperature in the TTL. On interannual timescales, both stratospheric and tropospheric modes of the large-scale variability could affect temperatures in the TTL. Here multiple linear regression (MLR) is used to investigate explained variance in the cold point tropopause temperature (CPT), cold point tropopause height (CPZ), 83 hPa water vapor (WV83), 83 hPa ozone (O₃83), and total cirrus cloud fraction with cloud base (TTLCCF) and top (ALLCF) above 14.5 km, all averaged over 15°S–15°N. Predictors of the MLR are a set of stratospheric and tropospheric large-scale modes of variability. The MLR explains significant variance in CPT (76%), CPZ (78%), WV83 (65%), O₃83 (62%), TTLCCF (52%), and ALLCF (36%). The interannual variability of CPT and WV83 is dominated by stratospheric processes associated with the Quasi-Biennial Oscillation (QBO) and Brewer-Dobson Circulation (BDC), whereas the variability of CPZ, O₃83, TTLCCF and ALLCF is also controlled by 500 hPa temperature (T500). Residual variability in CPT and CPZ not captured by the MLR are further significantly correlated to stratospheric temperature. It is shown that the portion of the BDC's shallow branch missed by the eddy heat flux based BDC index contributes significant amounts of the explained variances.

Plain Language Summary Between the tropical upper troposphere and lower stratosphere, water can exist as either vapor or ice. The amount of water that enters the stratosphere depends on the portion of vapor that is frozen out by the coldest temperature that air experiences in this region, which on interannual timescales could be modulated by both large-scale stratospheric and tropospheric modes of variability. Here we show that 76%, 65%, and 52% of the interannual variance in cold point temperature, water vapor at 83 hPa, and ice cloud fraction in this region can be explained using a multiple linear regression (MLR), where the predictors are the modes of the large-scale variability. Stratospheric processes are much more important in controlling the interannual variance of cold point temperature and water vapor at 83 hPa, but notably, the height of the cold point is controlled by both stratospheric and tropospheric processes. Residual variability of the cold point temperature not captured by the MLR is still connected to temperature variability in the stratosphere.

1. Introduction

The tropical tropopause layer (TTL) is a transition layer between the tropical troposphere and stratosphere and extends from the level of zero net radiative heating to the maximum height where clouds still exist (~14.5–~18.5 km) (e.g., Fu et al., 2007; Fueglistaler et al., 2009; Gettelman et al., 2004). A crucial component of the TTL is the water vapor and ice that exists there. Water vapor in the TTL can transit into the stratosphere, where it has significant impacts on Earth's radiation budget and stratospheric ozone (Ding & Fu, 2018; Flury et al., 2012; Forster and Shine, 1999; Fueglistaler & Haynes, 2005; Joshi et al., 2010; Kirk-Davidoff et al., 1999; Mote et al., 1996; Randel & Park, 2019; Solomon et al., 2010). Ice in this region exists as thin and extensive cirrus referred to as TTL cirrus clouds. These clouds can impact the TTL's local radiative heating rate, which may influence the upwelling and temperatures in the TTL (Corti et al., 2006; Dinh et al., 2010; Fu et al., 2018; McFarquhar et al., 2000; Wang & Fu, 2021; Yang et al., 2010). These cirrus clouds might also contribute a warming effect on the surface (Zhou et al., 2014). Despite their importance, climate models have difficulty simulating stratospheric water vapor concentrations and TTL cirrus clouds (Gettelman et al., 2009, 2010; Hardiman et al., 2015; Randel & Jensen, 2013; Wang & Fu, 2021).

The water vapor going into the stratosphere is largely regulated by the coldest temperatures that air experiences in the TTL, especially during boreal winter (Holton & Gettelman, 2001). Cold temperature anomalies in the TTL can largely limit the entry of water vapor into the stratosphere through the formation of TTL cirrus clouds (Flury

et al., 2012; Jensen et al., 1996, 2013; Randel & Jensen, 2013). Temperature variability in this region is a result of both stratospheric and tropospheric modes of large-scale variability (Charlesworth et al., 2019; Lu et al., 2020; Randel & Wu, 2015). Observed interannual variations in TTL temperature, water vapor, and clouds have been linked to stratospheric modes including the Quasi-Biennial Oscillation (QBO) and Brewer Dobson circulation (BDC) and tropospheric modes including the El Niño Southern Oscillation (ENSO) and Madden-Julian Oscillation (MJO) (Davis et al., 2013; Ding & Fu, 2018; Eguchi & Kodera, 2010; Li & Thompson, 2013; Liang et al., 2011; Sweeney et al., 2023; Tseng and Fu, 2017a, 2017b; Virts et al., 2010; Virts & Wallace, 2014; Ye et al., 2018). Based on both observational and modeling studies, wave activity on a variety of temporal and spatial scales can also impact TTL temperatures and cirrus clouds (Boehm & Verlinde, 2000; Grise & Thompson, 2013; Kim & Alexander, 2015; Podglajen et al., 2016; Kim et al., 2016; Podglajen et al., 2018; Chang & L'Ecuyer, 2020; Bramberger et al., 2022).

An open question remains to what extent these observed interannual variations are governed by stratospheric versus tropospheric processes (Ding & Fu, 2018; Fu, 2013; Garfinkel et al., 2013). This question is important because the decadal TTL variability has been linked to both (Garfinkel et al., 2013; Lu et al., 2020; Solomon et al., 2010; Xie et al., 2014). The different sources of variability may involve common mechanisms, for example, modulation of the TTL upwelling, complicating the partitioning of the sources (Austin & Reichler, 2008; Lin et al., 2017). This question is also important because connections between TTL variables and the modes of large-scale variability found in observations may help validate models' representation of the TTL. This study attempts to shed light on this question by examining key target variables in the TTL like temperature, water vapor, ozone, and cloud fraction observed from radio occultations, the Microwave Limb Sounder aboard the Aura satellite, and the CALIOP instrument. The explained variance of these target variables is investigated by employing a multiple linear regression (MLR) where predictors are the QBO, BDC, T500, and MJO (Dessler et al., 2013, 2014; Tseng & Fu, 2017a; Wang et al., 2019).

2. Data

2.1. Target Variables

2.1.1. Temperature

Temperature data come from Radio Occultation (RO) profiles from the COSMIC-1 and 2 as well as the MetOp-A, B, and C satellites, archived at the University Corporation for Atmospheric Research (Anthes et al., 2008; Schreiner et al., 2020). Data was preprocessed using the level 2 WetPrf product from June 2006 to December of 2021 (Sweeney & Fu, 2021). These RO temperature profiles have high accuracy and high vertical resolution (~0.5 km) in the TTL, but coarser horizontal resolution of about 200 km (Kuo et al., 2004; Kursinski et al., 1997; Zeng et al., 2019). The vertical temperature gradient and cold point tropopause temperature and height are also calculated from the RO temperature data.

2.1.2. Clouds

Cloud fraction data comes from the Cloud-Aerosol Lidar with Orthogonal Polarization (CALIOP) instrument aboard the CALIPSO satellite (Winker et al., 2010). CALIOP can provide information of cloud layers with optical depth as small as 0.01 or less, ideal for TTL cirrus cloud identification. We use the Level 2 V4.2 5-km Merged Layer Products from June of 2006 to December of 2021, using only nighttime measurements to avoid solar contamination of the lidar signals (Thornberry et al., 2017; Thorsen et al., 2013). Cloud fraction is derived from the lidar data as the number of detections of a cloud divided by the total number of observations in each $2.5^\circ \times 2.5^\circ$ grid cell at a given level. Positive cloud identifications require Cloud-Aerosol Distinction (CAD) values of greater than 30. This study uses an adapted version of the Level 2 V4.2 data for clouds above the lapse rate tropopause (Sweeney et al., 2023; Tseng & Fu, 2017b).

Two different categories of clouds are identified in this study: clouds with bases above 14.5 km (TTL cirrus) and clouds with tops above 14.5 km and no constraint on their base height (All clouds). The 14.5 km altitude is approximately the level of zero net radiative heating in the tropical atmosphere (Fu et al., 2007; Gettelman et al., 2004; Tseng & Fu, 2017a). We consider TTL cirrus and All clouds separately because TTL cirrus clouds are more relevant for the dehydration of the TTL, while All clouds are more relevant for the total energy budget of the tropics (Corti et al., 2006; Jensen et al., 2013; Sokol & Hartmann, 2020; Sweeney et al., 2023).

Both the TTL cirrus cloud fraction and All cloud fraction are turned into one-dimensional monthly timeseries referred to as TTLCCF and ALLCF respectively. TTLCCF measures total cloud fraction similarly to TTL cirrus cloud fraction described above but does not consider the vertical extent of the TTL cirrus cloud (i.e., only measures whether a TTL cirrus cloud is present, and not its vertical profile). ALLCF only measures whether a cloud top above 14.5 km is present, and not the vertical profile of the cloud.

2.1.3. Water Vapor and Ozone

Water vapor and ozone data come from the Microwave Limb Sounder (MLS) onboard the Aura Satellite (Read et al., 2007). MLS measurements began in August 2004 and continue until present day. Water vapor and ozone mixing ratios come from monthly mean Level 3 version 5 MLS data from June 2006 to December of 2021 (Livesey et al., 2021). Tropical lower stratospheric water vapor is primarily sourced from the troposphere, and transits slowly upward from the tropopause (Randel & Park, 2019). Because we are particularly interested in the interannual variability of lower-stratospheric water vapor, all water vapor data is lagged by 1 month to account for the slow transit time into the lower stratosphere.

2.2. Predictors

2.2.1. Quasi-Biennial Oscillation (QBO) Index

The QBO is the main mode of the large-scale variability in the tropical stratosphere (Baldwin et al., 2001) and is a stratospheric process. The QBO index is defined using the monthly mean 50 hPa zonal wind averaged over 10°S–10°N from ERA5 (Hersbach et al., 2020). We let the QBO index lead the TTL variables by 2 months to account for the QBO temperature anomaly's descent to the cold point tropopause (Dessler et al., 2013, 2014; Ding & Fu, 2018; Tian et al., 2019; Tseng & Fu, 2017a; Ye et al., 2018).

2.2.2. Madden Julian Oscillation (MJO) Index

The MJO is the dominant mode of intraseasonal variability in the tropical atmosphere and is a tropospheric process (Madden & Julian, 1971). The MJO index used here is the second principal component of the velocity potential index (Ventrice et al., 2013). Maximums in this MJO index are associated with peak MJO-related convection over the western Pacific and suppressed convection over the eastern Indian Ocean (Tseng & Fu, 2017a; Virts & Wallace, 2014). We use the velocity potential index provided by the NOAA Physical Science Laboratory (<https://www.psl.noaa.gov/mjo/mjoindex/>).

2.2.3. Temperature at 500 hPa (T500)

The 15°S–15°N 500 hPa temperature (T500) from the ERA5 reanalysis measures tropospheric temperature. ENSO is the dominant mode of tropospheric temperature variability (Philander, 1990). T500 is highly correlated with a 3-month lead of the ENSO MEIv2 index ($r = 0.73$) and thus implicitly captures much of the ENSO variability (Dessler et al., 2013; Marsh & Garcia, 2007; Wang et al., 2019). T500 can impact the TTL through longwave heating, changing tropical convective activity, and other processes (Lin et al., 2017; Ye et al., 2018). Increases in T500 can dynamically induce upwelling in the TTL through the eddy momentum flux convergence in the tropical upper troposphere driven by convective latent heat (Boehm & Lee, 2003; Deckert & Dameris, 2008; Garny et al., 2011), which has been considered part of the BDC in some studies (e.g., Boehm & Lee, 2003) but not in others (e.g., Wu & Zheng, 2022). T500 thus impacts the TTL through both thermodynamic and dynamic processes and is considered a tropospheric process here.

2.2.4. Eddy Heat Flux Based Brewer-Dobson Circulation Index (BDC_{EHF})

The BDC influences TTL variability by modulating the TTL upwelling (Haynes et al., 1991; Holton et al., 1995; Yulaeva et al., 1994). The deep branch of the BDC is driven by extratropical stratospheric waves, which is linked to the meridional eddy heat flux in the lower stratosphere (Li & Thompson, 2013). To quantify the BDC deep branch, we calculate the monthly averaged zonal mean meridional eddy heat flux at 100 hPa averaged over 25°–90° in the northern hemisphere minus that of the southern hemisphere (Randel et al., 2002; Tseng & Fu, 2017a). We refer to this BDC index based on the eddy heat flux as BDC_{EHF} . Temperatures are correlated with wave driving during the current and previous months; thus, the BDC_{EHF} index is created using a 3-month running mean centering on the previous month (Fu et al., 2015; Li & Thompson, 2013; Lin et al., 2009; Tseng & Fu, 2017a). This BDC_{EHF} index is calculated using 6 hourly ERA5 data from 2006 to 2021. Note that in addition

to the BDC deep branch, the eddy heat flux-based index BDC_{EHF} may also include a portion of the shallow branch of the BDC (Grise & Thompson, 2013).

2.2.5. Partial Shallow Branch of the Brewer-Dobson Circulation Index (BDC_{PSB})

In addition to extratropical stratospheric waves, tropical and subtropical waves also drive the TTL upwelling. The upwelling due to the subtropical waves is associated with the shallow branch of the BDC (Abalos et al., 2014; Grise & Thompson, 2013; Orland & Alexander, 2014). The shallow branch of the BDC thus also influences TTL variability by modulating the TTL upwelling. Note that in this study, the upwelling driven by equatorial planetary waves (Boehm & Lee, 2003; Deckert & Dameris, 2008; Garny et al., 2011), which is related to T500, is not considered as part of the BDC. We attempt to quantify the role of the shallow branch that may be missed by the BDC_{EHF} by using the residual TTL upwelling after removing the impacts of the QBO, T500, and BDC_{EHF} . This residual TTL upwelling represents a portion of the shallow branch of the BDC which is not included in BDC_{EHF} ; thus, we refer to it as the partial shallow branch of the BDC (BDC_{psb}).

To quantify the TTL upwelling, we calculate the upwelling at 100 hPa over 15°S–15°N using the transformed Eulerian mean (TEM) vertical velocity, for 2006–2021 using the 6-hourly ERA5 reanalysis following Equation 1 (e.g., Abalos et al., 2012; Haynes et al., 1991; Randel et al., 2008; Rosenlof, 1995).

$$\overline{w^*} = \overline{w} + \frac{1}{a \cos \varnothing} \frac{\partial}{\partial \varnothing} \left(\cos \varnothing \frac{\overline{vT'}}{S} \right) \quad (1)$$

where $\overline{w^*}$ is the zonal mean TEM residual vertical velocity, \overline{w} is the zonal mean vertical velocity from ERA5, a is the radius of the earth, v is the meridional velocity, T is the temperature, and S is the stability parameter $S = \frac{HN^2}{R}$, a function of the Brunt-Vaisala frequency (N), with $H = 7$ km and $R = 287 \text{ m}^2\text{s}^{-2}\text{K}^{-1}$. Overbars and primes represent zonal means and zonal deviation respectively. After computing the upwelling, we regress out the combined impact of the QBO, T500, and BDC_{EHF} using a MLR (Abalos et al., 2014; Garfinkel & Hartmann, 2008). The 100 hPa upwelling before regressing out QBO, T500 and BDC_{EHF} has a correlation coefficient of -0.32 , 0.49 , and 0.46 , respectively, with the QBO, T500 and BDC_{EHF} (the MLR using the QBO, BDC_{EHF} , and T500 can explain 60% of the variability in the raw 100 hPa upwelling).

Because this study focuses on interannual variability, all data is deseasonalized and detrended. The target variables and predictors are created as the monthly anomalies by removing the monthly climatology from June 2006 to December 2021. Before removing linear trends in each timeseries, trends are computed using linear regression and are provided in Table S1 in Supporting Information S1. No trend is significant at the 95% confidence level besides that of the ALLCF timeseries, but this trend is not further investigated here.

3. Results

The climatology and interannual standard deviation of tropical upper-tropospheric and lower-stratospheric temperature, water vapor, vertical temperature gradient, and cloud fractions from June 2006 to December 2021 are provided in Figure S1 in Supporting Information S1. Importantly, the interannual variability for all these variables maximizes within 15°S–15°N. A significant cloud fraction variance occurs above the climatological cold point tropopause (Figures S1i and S1j in Supporting Information S1). Cloud fraction variability above the climatological cold point tropopause may be related to coincident changes in tropopause height. Figures S1 k–l in Supporting Information S1 show the interannual variance in a vertical coordinate relative to the cold point tropopause height, showing cloud fraction variability to maximize below the cold point tropopause.

3.1. Target Variable Correlations With Modes of Large-Scale Variability

Figure 1 shows the correlation between target variables with the zonal mean cold point tropopause temperature (CPT) averaged over 15°S–15°N (row 1), and the correlations of target variables with the modes of large-scale variability (row 2–6). Although the CPT is not a mode of variability, it is critically important for stratospheric water vapor (e.g., Randel & Jensen, 2013) and is highly correlated with TTL cirrus cloud fraction (Tseng & Fu, 2017a). CPT is significantly correlated with stratospheric temperatures but has little correlation with those in the troposphere (Figure 1a), suggesting that processes controlling the CPT also impact the tropical lower stratosphere (Randel & Wu, 2015). Note that tropospheric processes may still impact the CPT with competing effects

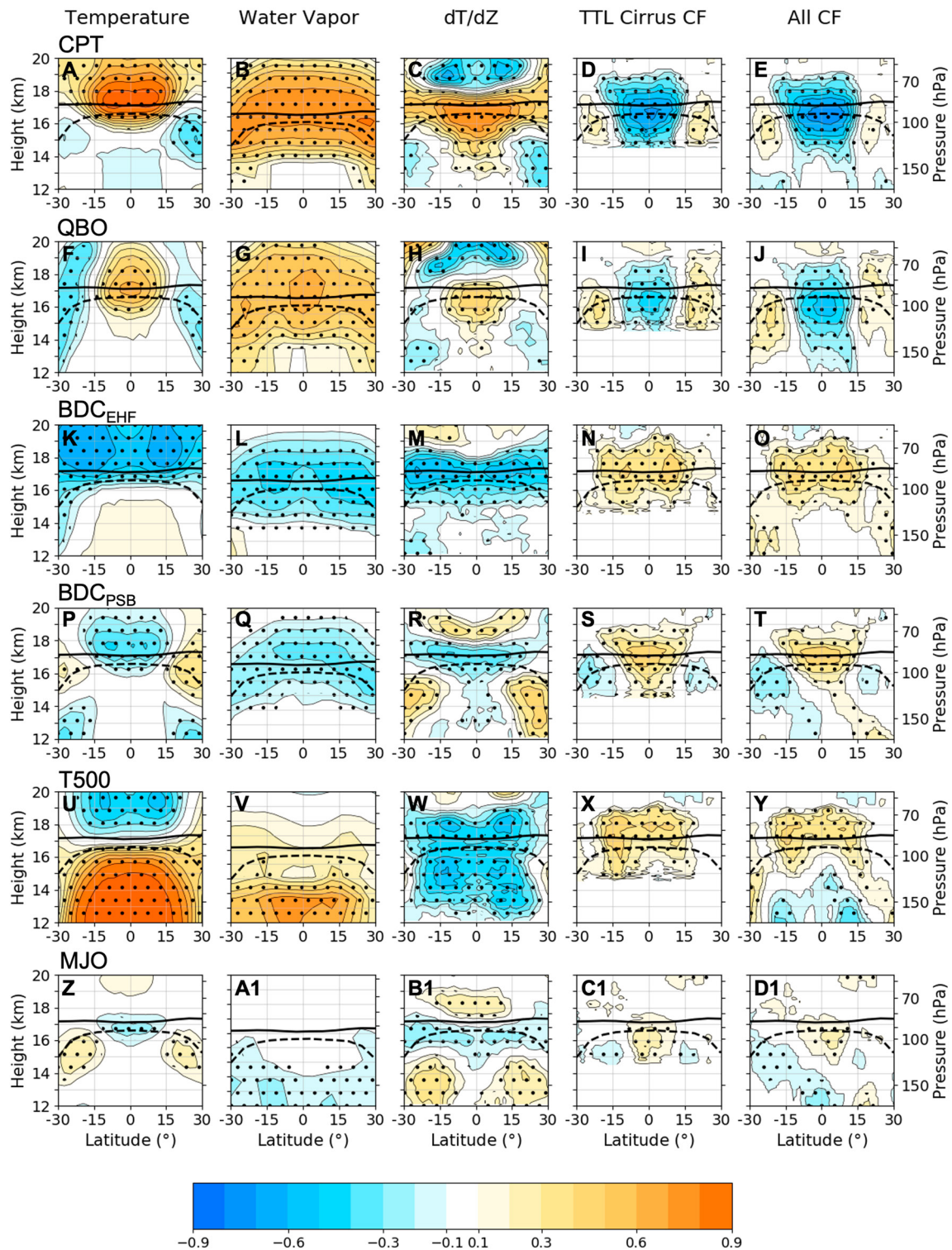


Figure 1. Correlations in tropical upper troposphere and lower stratosphere between target variable monthly anomalies and modes of the large-scale variability, except for row 1 that shows correlation between target variables and cold point temperature (CPT) averaged over 15°S–15°N. Stippling indicates significance at 95% confidence and the solid (dashed) black line is the climatological mean cold point (lapse rate) tropopause.

canceling much of the correlation between CPT and tropospheric temperatures. Lower-stratospheric water vapor reaches correlations of ~ 0.8 at the cold point tropopause (Figure 1b), indicative of the temperature control of lower-stratospheric water vapor. Water vapor is transported vertically into the stratosphere over the tropics by the BDC (Brewer, 1949; Flury et al., 2012, 2013; Mote et al., 1996), and is also transported between lower and higher latitudes through quasi-horizontal isentropic mixing (Randel & Park, 2019). These processes are responsible for the convex shape of peak correlations between CPT and water vapor in the TTL (Figure 1b). CPT is strongly anticorrelated with equatorial TTL cirrus and All cloud fraction (Figures 1d and 1e). Positive correlations between CPT and cloud fraction exist near the subtropical lapse rate tropopause, the inverse of the correlation between CPT and subtropical temperature. The strong correlations between CPT and the target variables stress the temperature control of the water partitioning between vapor and clouds in the TTL. Correlations between the CPT and target variables extends to higher latitudes in Figure S2 in Supporting Information S1.

The QBO and temperature are correlated in the equatorial TTL, but anticorrelated in the subtropical TTL due to the QBO's meridional circulation (Figure 1f) (Baldwin et al., 2001; Pahlavan et al., 2021; Plumb & Bell, 1982). QBO correlations with cloud fraction are inverse to those of temperature (Figures 1i and 1j). Subtropical cloud fraction correlations are weaker than the equatorial signal, possibly due to the weaker QBO-temperature correlations and the lower relative humidity. Significant QBO correlations with All cloud fraction reach into the troposphere as low as ~ 13 km (Figure 1j), below the region of peak QBO power (Sweeney et al., 2023). This deep QBO signature may be due to convective feedbacks (Tegtmeier et al., 2020). The QBO and water vapor correlations peak at the equatorial tropopause and are spread latitudinally due to quasi-isentropic mixing (Figure 1g). The QBO impacts lapse-rate tropopause temperature out to near 50° in both hemispheres with weak statistically significant implications for cloud fraction (Figure S2 in Supporting Information S1).

Increases in BDC_{EHF} cause upwelling and cooling in the tropical lower stratosphere (Figure 1k) (Mote et al., 1996; Plumb & Eluszkiewicz, 1999; Randel et al., 2002). Decreasing temperature and vertical temperature gradient promotes cloud formation at and above the climatological mean tropopause (Figures 1n-o). Notably, temperature and CPT correlations can be largely inferred from temperature and QBO minus temperature and BDC_{EHF} , both in the TTL (i.e., Figure 1a resembles Figure 1f minus Figure 1k), and globally (Figure S2 in Supporting Information S1).

The BDC_{PSB} index is related to TTL cold anomalies flanked by subtropical upper-tropospheric warm anomalies (Figure 1p), with tropospheric cold anomalies underneath the warm anomalies. BDC_{PSB} is also anticorrelated with lower-stratospheric water vapor (Figure 1q). BDC_{PSB} cloud fraction correlations peak near the equatorial tropopause (Figures 1s-t). The BDC_{PSB} and temperature correlation pattern resembles the temperature tendencies caused by subtropical upper-tropospheric waves which can cause subseasonal variability in the shallow branch of the BDC (Abalos et al., 2014; Grise & Thompson, 2013). The shallow branch of the BDC is also driven by subtropical stratospheric waves, which is considered in BDC_{EHF} (Grise & Thompson, 2013). Figures 1p-t show that BDC_{PSB} is well correlated with the target variables and is an important component of TTL variability.

T500 measures tropospheric temperature and is positively correlated with temperatures below the tropopause (Figure 1u). Increased T500 dynamically induces upwelling and cooling of the lower stratosphere (Calvo et al., 2010; Lin et al., 2017; Randel et al., 2009; Shepherd & McLandress, 2011). The net result of warming below the tropopause and cooling above is a reduction of vertical temperature gradient throughout the TTL (Figure 1w). T500 has significant correlations with cloud fraction near and above the climatological tropopause (Avery et al., 2017; Davis et al., 2013; Ye et al., 2018). The correlation between T500 and lower-stratospheric water vapor is insignificant (Figure 1v), consistent with T500's weak impact on CPT ($r = -0.11$) (Diallo et al., 2018; Garfinkel et al., 2021; Konopka et al., 2016; Liang et al., 2011; Ziskin Ziv et al., 2022). This may be expected given that much of the T500 variability is related to ENSO which shows a strong longitudinal dipole impact on CPT which cancels in the zonal mean (Garfinkel et al., 2021; Randel et al., 2000; Scherllin-Pirscher et al., 2012; Tseng & Fu, 2017a). Interpreting the physical mechanism by which T500 influences the CPT is complicated due to competing processes, but it is important to understand the response of stratospheric water vapor to global warming. Discussion of the relevant mechanisms by which T500 may impact the TTL is provided in Section 3.3. The correlation between T500 and global temperature (Figure S2 in Supporting Information S1) reveals a meridional circulation in the tropical and subtropical lower stratosphere.

The last row in Figure 1 shows correlations between the MJO and target variables. The MJO is the main mode of intraseasonal variability in the tropics (Madden & Julian, 1971), and impacts subseasonal variability of temperature

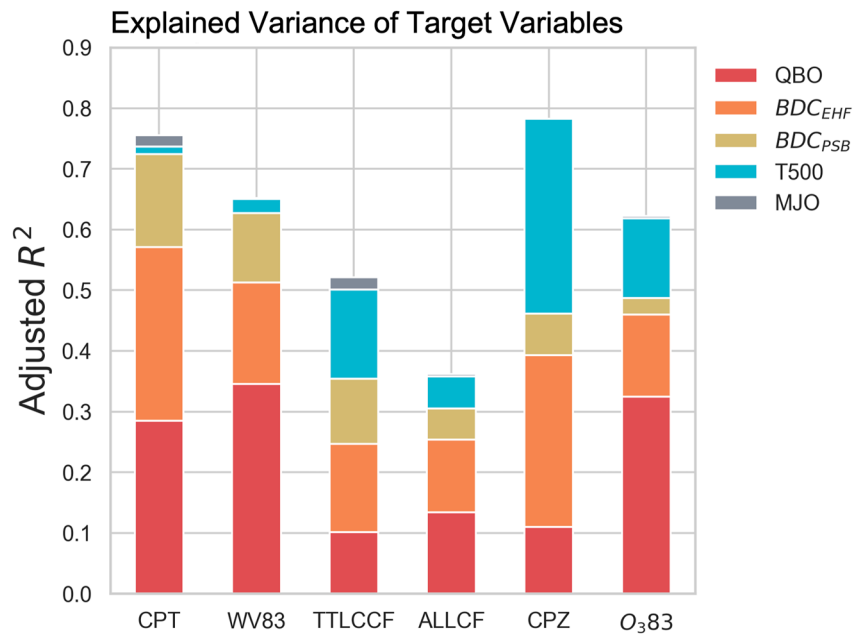


Figure 2. Adjusted R^2 from multiple linear regression model applied to target variables using modes of the large-scale variability as predictors. Colored sections indicate the estimated contribution to the adjusted R^2 from each predictor.

and cloud fraction in the TTL (Virts et al., 2010; Virts & Wallace, 2014). MJO-temperature correlations have a distinct pattern of weak equatorial (subtropical) anticorrelation (correlation) (Grise & Thompson, 2013). Results of Figure 1 show that the MJO only weakly correlates with the TTL target variables. This is partly because the monthly averaging of the MJO index and target variables smooths the intraseasonal variability.

3.2. Explained Variances in Target Variables From MLR

We next use the modes of the large-scale variability as predictors in a multiple linear regression (MLR) to quantify the explained variance of cold point tropopause temperature (CPT), water vapor at 83 hPa (WV83), cold point tropopause height (CPZ), ozone concentrations at 83 hPa (O_383), total TTL cirrus cloud fraction (TTLCCF), and All cloud fraction (ALLCF), all averaged over $15^{\circ}S$ - $15^{\circ}N$.

Explained variance is quantified using the adjusted R^2 , which accounts for artificial inflation due to collinearity in the MLR and is always smaller than the true R^2 . The unique contribution of explained variance to the adjusted R^2 from each predictor is not possible unless predictors are independent of each other. A correlation matrix among all predictors and target variables is provided in Figure S3 in Supporting Information S1. The predictors show small correlations with each other over the period investigated, which are all statistically insignificant. For example, the correlation is -0.07 between QBO and BDC_{EHF} , and 0.14 between T500 and BDC_{EHF} . To account for these non-zero correlations, we partition the adjusted R^2 into the unique contributions from the QBO, BDC_{EHF} , BDC_{PSB} , T500, and MJO by recursively adding each predictor to our MLR model while also permuting the order of addition. This allows for an estimate of unique explained variance (Lindeman et al., 1980). We note that this method is not perfect because the predictors are not entirely independent but provides an estimate of the unique explained variance from each mode of variability.

Figure 2 shows the MLR's explained variance of CPT (76%), WV83 (65%), TTLCCF (52%), ALLCF (36%), CPZ (78%), and O_383 (62%). Stratospheric processes (i.e., the QBO, BDC_{EHF} , and BDC_{PSB}) dominate the variance captured in CPT, WV83, and ALLCF. BDC_{PSB} explains substantial variances in CPT, WV83, and TTLCCF, and including BDC_{PSB} increases the explained variance of CPT and TTLCCF compared to previous studies (e.g., Tseng & Fu, 2017a). BDC_{PSB} should therefore be considered as an important component of the TTL variability. Tropospheric processes (i.e., T500 and the MJO) are of lesser importance, although T500 is a significant contribution to TTLCCF and O_383 variability and contributes nearly half of the variance in CPZ. The MJO minimally affects any target variable.

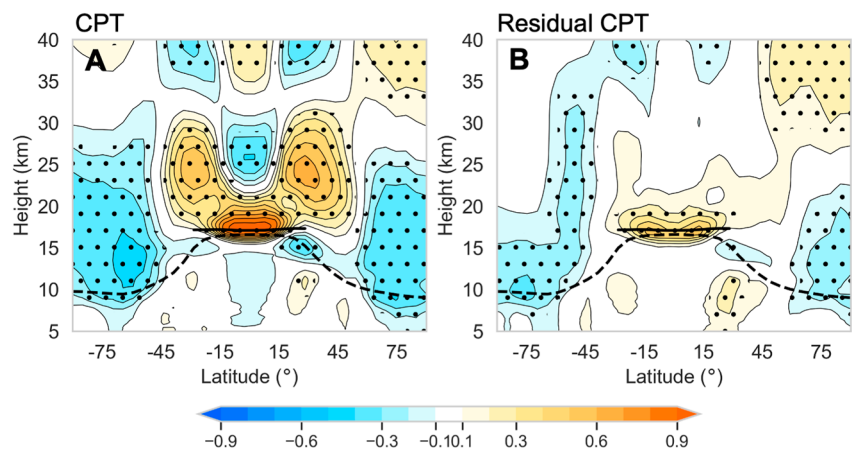


Figure 3. Correlation of zonal mean temperature globally from 5 to 40 km with (a) cold point temperature averaged over 15°S-15°N (CPT), and (b) residual CPT after regressing out all modes of large-scale variability using the MLR shown in Figure 2. Stippling indicates significance at 95% confidence and the solid (dashed) black line is the climatological mean cold point (lapse rate) tropopause.

Tseng and Fu (2017a) stressed the importance of CPT for TTLCCF variability. A linear regression using only CPT as a predictor explains 41% of TTLCCF variance, while the MLR in Figure 2 explains 52%. Including CPT as an additional predictor in the MLR for TTLCCF only increases the explained variance slightly from 52% to 54%, indicating that most of the CPT control of TTLCCF has already been included in our MLR. But this is not true for WV83 whose explained variance increases by 8% (from 65% to 73%) when including CPT as an additional predictor. Thus, a better understanding of the CPT variance would help explain WV83 variance. The cloud fraction explained variance is strongly dependent on altitude, where at 17 km the MLR explains over 60% of the variance in TTL cirrus and All cloud fraction, possibly due to the higher frequency of laminar tropopause cirrus at these altitudes (Wang et al., 2019).

TTL ozone variability is primarily due to the TTL upwelling and in-mixing of ozone depleted tropospheric air (Konopka et al., 2009; Randel et al., 2007; Solomon et al., 2016; Wang and Fu, 2021, 2023). Long-term ozone concentrations at a fixed height in the TTL may decrease due to the strengthening of the tropical upwelling associated with the BDC, and/or tropospheric expansion due to warming (Banerjee et al., 2016; Chiodo et al., 2018; Garcia & Randel, 2008; Lin & Fu, 2013; Match & Gerber, 2022; Wang et al., 2019). Figure 2 shows that the MLR explains 62% of O_3 83 variance, with about half attributed to the QBO while the rest is split roughly equally between BDC_{EHF} and T500. Despite the QBO's important role in determining O_3 83, decadal changes in O_3 83 due to the QBO are uncertain due to ambiguity in the QBO response to global warming (e.g., Butchart et al., 2020; Fu et al., 2020; Richter et al., 2020). Our results agree with previous work and suggest that both T500 and the BDC_{EHF} affect O_3 83 (Match & Gerber, 2022). However, the T500 influence on O_3 83 may operate via a dynamic response in the TTL upwelling. Further discussion on T500's impact on target variables including O_3 83, can be found in Section 3.3.

A key result of Figure 2 is that despite the strong correlation between CPT and CPZ ($r = -0.74$) the interannual variability of CPT is predominately explained by stratospheric processes, while CPZ's variability is equally explained by stratospheric and tropospheric processes. In Figure 3, we further examine how CPT covaries with the tropospheric and stratospheric temperatures. Figure 3a illustrates the correlations of zonal mean temperature from 5 to 40 km over 90°S-90°N obtained from the RO data with CPT. Figure 3b shows the correlations of zonal mean temperature and the residual CPT after removing all variance captured by the MLR in Figure 2.

CPT is strongly correlated with temperatures throughout the global stratosphere, but not with those of the troposphere, as seen in Figure 3a, consistent with the dominant role of stratospheric processes in CPT variance. The checkerboard pattern in the tropical stratosphere is due to the QBO's meridional circulation (Baldwin et al., 2001). The out of phase correlation above the equatorial cold point and the polar lower stratosphere is due to the BDC's meridional circulation. Regressing the modes of large-scale variability out of the CPT significantly reduces its covariability with stratospheric temperatures (Figure 3b).

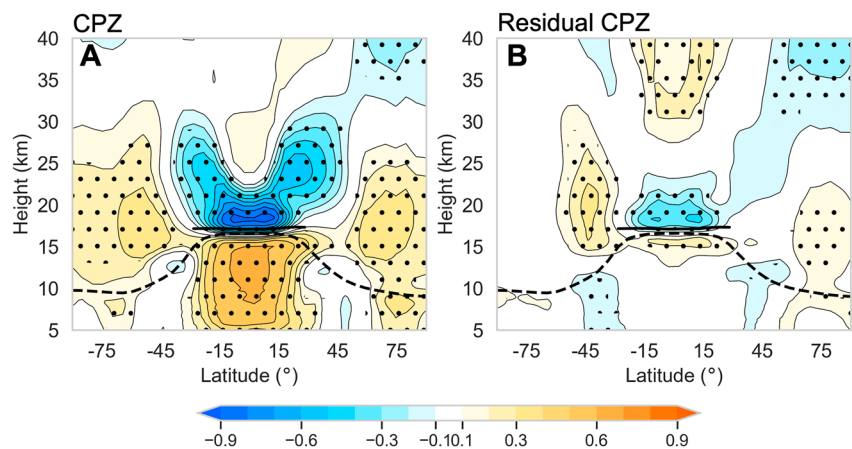


Figure 4. Same as Figure 3, but for cold point tropopause height (CPZ).

Figure 3b shows that residual CPT is still correlated (anticorrelated) near the equatorial tropopause (polar lower stratosphere). This correlation pattern with the residual CPT is reminiscent of the global correlations expected from the BDC, which is surprising given that the QBO, BDC_{EHF} , BDC_{PSB} , T500, and MJO have all been regressed out. Note that both the CPT variability and that of zonal mean temperature throughout the global upper troposphere and lower stratosphere are derived from RO data, whereas the BDC_{EHF} and BDC_{PSB} indices are derived from ERA5 (see Section 2.2). Thus, this pattern of residual variability may be partly caused by reanalysis errors in representation of the BDC.

Figure 4 shows the correlations between zonal mean temperature with CPZ. In contrast to CPT, the CPZ is also highly correlated with temperature in the tropical troposphere (Figure 4a). Increased tropospheric temperatures raise CPZ through thermal expansion of the troposphere in addition to dynamical upwelling. T500 contributes to nearly half of the interannual variance in CPZ (see Figure 2), which is relevant for future increases in the CPZ in response to the T500 increase (Lorenz & DeWeaver, 2007; Santer et al., 2003). The stark differences in correlation patterns of CPT versus that of CPZ (Figures 3a and 4a) may help validate model representations of tropical tropopause characteristics. After regressing out all modes of variability from CPZ the correlation patterns with temperature are still connected to the global stratosphere (Figure 4b), which again indicates a potential issue in the indices used to represent the stratospheric processes.

3.3. Isolating the Role of the TTL Upwelling and Thermodynamics

The large-scale modes used as predictors in this study can impact TTL variability by modulating the TTL upwelling. This upwelling helps shape temperatures of the region through adiabatic cooling and, to a smaller extent, cloud formation and the transport of radiatively active species (Abalos et al., 2012; Birner & Charlesworth, 2017; Corti et al., 2006). On the other hand, T500 could also impact the TTL through thermodynamic processes in addition to upwelling. Here we examine the role of the dynamic upwelling and thermodynamic processes.

To assess the upwelling's impact on TTL variability, we use the original 100 hPa TEM upwelling from 15°S to 15°N as described in Section 2.2. Correlations between this index and the target variables are shown in Figures 5a–5e. The 100 hPa upwelling is positively correlated with tropospheric temperatures and negatively correlated with lower-stratospheric temperatures (Figure 5a). The 100 hPa upwelling is strongly anticorrelated with CPT ($r = -0.68$) and is also anticorrelated with TTL water vapor (Figure 5b). Upwelling also increases cloud fractions (Figures 5d and 5e), mediated by the reductions in near tropopause temperature and vertical temperature gradient (Figures 5a and 5c). TTLCCF has a correlation with the 100 hPa upwelling of $r = 0.69$. Thus, regressing only this upwelling onto TTLCCF can explain 47% of the variability, close to what the MLR with all predictors can (52% shown in Figure 2). Since most of the TTLCCF variance captured by the full MLR is explained using just the 100 hPa upwelling, it is suggested that the modes of the large-scale variability control TTL cirrus clouds by modulating the 100 hPa upwelling.

Temperature and 100 hPa upwelling correlations in Figure 5a are reminiscent of temperature and T500 correlations shown in Figure 1u, but with stronger (weaker) correlations in stratosphere (troposphere). T500 is well

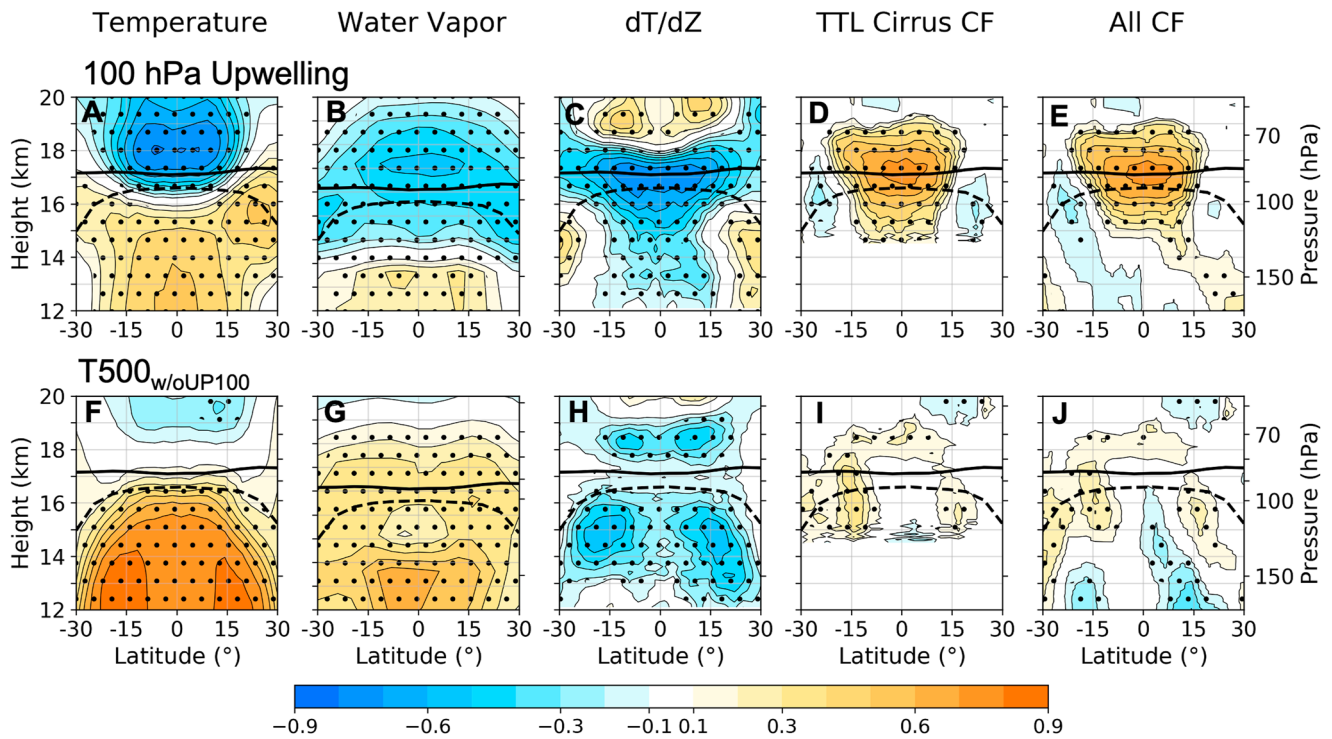


Figure 5. As Figure 2 but A-E show correlations of target variables with the 100 hPa upwelling. F-J shows correlations with $T500_{w/oUP100}$ (i.e., $T500$ after regressing out the 100 hPa upwelling, QBO, and BDC_{EHF}).

correlated with the 100 hPa upwelling ($r = 0.49$) and can influence the target variables by modulating the upwelling. $T500$ may induce upwelling through eddy momentum flux convergence in the tropical upper troposphere driven by convective latent heating (Boehm & Lee, 2003). However, $T500$ may also impact the target variables through thermodynamic processes such as radiative heating of the TTL, tropical tropospheric expansion, tropical convection, and/or other physical processes (Lin et al., 2017). We next attempt to isolate the $T500$ thermodynamic effects using regression analysis. It might be difficult to do so by just using the regression analysis given that the dynamic and thermodynamic processes may be closely coupled, yet this analysis may still provide valuable insights. We urge further modeling studies to validate results shown here.

To remove $T500$'s dynamic contribution to TTL variability, we regress the 100 hPa upwelling out of $T500$. In addition to the 100 hPa upwelling, the QBO and BDC_{EHF} indices are also removed from $T500$. Since the impact of removing the QBO and BDC_{EHF} is small due to minimal correlations with $T500$ (Figure S3 in Supporting Information S1), we refer to this $T500$ index without the dynamic components as $T500_{w/oUP100}$ (which can be considered as the $T500$ thermodynamic index). Figures 5f–5j show the correlation coefficients between $T500_{w/oUP100}$ with target variables. Figure 5f shows warming below the tropopause and little to no cooling in the stratosphere as would be expected after removing the dynamically induced response to $T500$. While significant positive tropospheric temperature correlations in Figure 5f reach closer to the equatorial cold point tropopause than those with the original $T500$ index shown in Figure 1u, no statistically significant correlation between $T500_{w/oUP100}$ and CPT exists ($r = 0.15$). Given that the 100 hPa upwelling explains most of the TTLCCF variability, removing its influence from $T500$ also largely removes its influence on TTL cirrus clouds (Figures 5i and 5j).

Notably, $T500_{w/oUP100}$ shows a significant correlation with lower-stratospheric water vapor (Figure 5g). This is in stark contrast to results of Figure 1v, where the $T500$ index showed no significant impact on lower-stratospheric water vapor. Figure 5g may suggest that $T500_{w/oUP100}$ covaries with lower-stratospheric water vapor, but this covariability is damped by coincident cooling due to the TTL upwelling caused by $T500$. While $T500_{w/oUP100}$ is correlated with lower-stratospheric water vapor, it is not significantly correlated with CPT. Thus, the $T500_{w/oUP100}$ impact on lower-stratospheric water vapor might not work through a simple increase in CPT but may instead be related to $T500_{w/oUP100}$'s impact on the TTL environment where dehydration, convective evaporation, subtropical

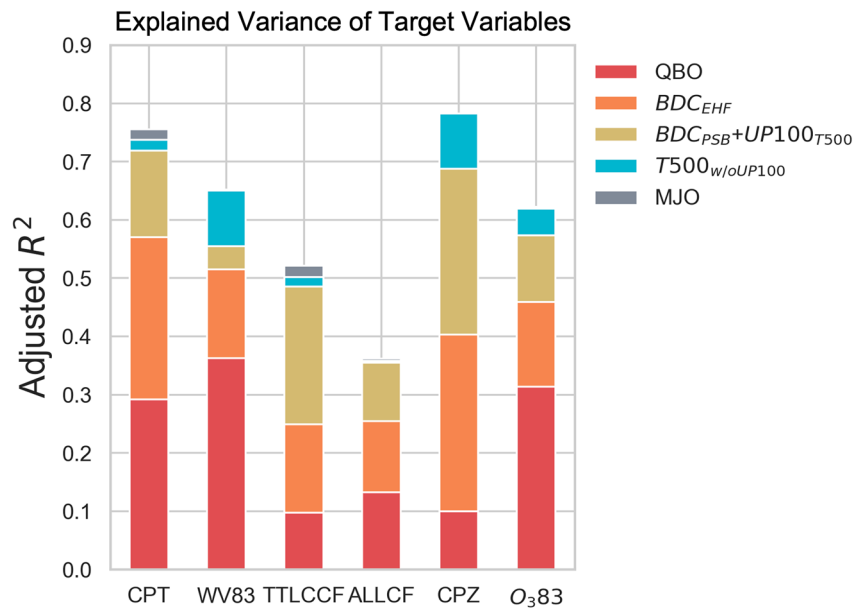


Figure 6. Same as Figure 2, but the $BDC_{PSB} + UP100_{T500}$ is the BDC_{PSB} without removing the influence of T500, that is, the contribution from BDC_{PSB} and the 100 hPa upwelling due to T500 ($UP100_{T500}$). $T500_{w/oUP100}$ is the T500 index after regressing out the original 100 hPa upwelling, the QBO, and BDC.

water vapor in-mixing, and/or other uninvestigated processes occur (Bourquet & Linz, 2023; Dessler et al., 2013; Ye et al., 2018).

The differences between Figures 1u-y and 5f-j suggest that T500 contributes to TTL variability partly through changes in the 100 hPa upwelling. Figure 6 is the same as Figure 2 but replaces T500 with $T500_{w/oUP100}$ and BDC_{PSB} with $BDC_{PSB} + UP100_{T500}$. $BDC_{PSB} + UP100_{T500}$ is the combination of BDC_{PSB} and the 100 hPa upwelling induced by T500, which is computed in the same way as BDC_{PSB} but without regressing out T500 (see Section 2.2). This replacement is to group the T500 that is linearly related to the 100 hPa upwelling ($UP100_{T500}$) with the BDC_{PSB} and then isolate the T500 that is not linearly related to the 100 hPa upwelling ($T500_{w/oUP100}$).

This replacement does not impact the total explained variance, and small changes in explained variances by QBO, BDC_{EHF} and MJO result from changes in collinearities. Figure 6 shows that $T500_{w/oUP100}$ contributes minimally to explained variance of TTLCCF and ALLCF because cloud fraction variance is tightly coupled to the TTL upwelling. While Figure 2 showed that T500 contributes nearly half of the explained variance in CPZ, Figure 6 shows that $T500_{w/oUP100}$ contributes much less to the explained variance in CPZ. Figures 2 and 6 suggest that more than 2/3 of the T500 control of CPZ is through T500's induced upwelling (Austin & Reichler, 2008). Similarly, only about 1/3 of explained O_{383} variance by T500 (Figure 2) comes from $T500_{w/oUP100}$ (Figure 6).

In contrast, Figure 6 shows an enhanced role of $T500_{w/oUP100}$ in WV83 variance relative to T500 in Figure 2. The $T500_{w/oUP100}$ influence on WV83 may be important for climate feedbacks due to the important role of lower-stratospheric water vapor (Solomon et al., 2010). Finally, it is worth noting that the explained CPT variances by BDC_{PSB} (Figure 2) and $BDC_{PSB} + UP100_{T500}$ (Figure 6) are almost identical, indicating that both $UP100_{T500}$ and $T500_{w/oUP100}$ have little impacts on CPT.

3.4. Seasonality

The seasonal influence of large-scale modes on TTL variability is less studied. Correlation between CPT and lower-stratospheric water vapor is strongest in boreal winter (Lu et al., 2020; Randel & Jensen, 2013; Randel & Park, 2019). Seasonal changes in the tropical upwelling and the Asian monsoon also impact TTL variability (Das & Suneeth, 2020; Randel et al., 2007, 2010; Sunilkumar et al., 2010; Ueyama et al., 2015, 2018; Walker et al., 2015). Modes of the large-scale variability may also impact the target variables differently throughout the year (Konopka et al., 2016; Li & Thompson, 2013; Martin et al., 2021; Sweeney et al., 2023; Tweedy et al., 2018).

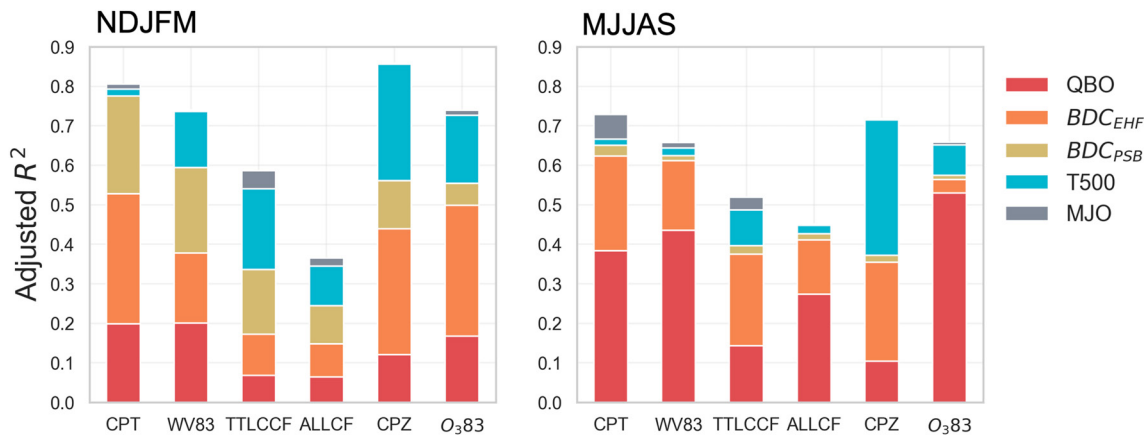


Figure 7. Adjusted R^2 from MLR model applied to target variables for NDJFM and MJJAS individually. Colored sections indicate the contribution to the adjusted R^2 from each predictor.

Here, we examine how these modes of variability impact the target variables during extended boreal winter (November–March; NDJFM) and extended boreal summer (May–September; MJJAS). During NDJFM the TTL is colder, drier, and has more TTL cirrus than in MJJAS (Figure S4 in Supporting Information S1). During MJJAS, lower stratospheric water vapor increases (Figure S4G in Supporting Information S1) and All cloud fraction maximizes (Figure S4J in Supporting Information S1) in the northern hemisphere TTL due to the Asian Summer Monsoon (e.g., Santee et al., 2017). Regardless of season, interannual variance is strongest near the equator (Figure S4 in Supporting Information S1).

The MLR used in Figure 2 is fit in both NDJFM and MJJAS individually in Figure 7. Figure S5 in Supporting Information S1 shows correlation matrices between all target variables and predictors for both NDJFM and MJJAS separately. The MLR predicts all target variables better during NDJFM than MJJAS, except ALLCF. Note that the partitioning of explained variance is less reliable after splitting the data based on season because of collinearities between the modes of variability, and smaller number of degrees of freedom.

Figure 7 highlights the increased QBO influence during MJJAS for all variables except CPZ: CPT ($r = 0.5$ in NDJFM and $r = 0.61$ in MJJAS), WV83 (0.53 in NDJFM and 0.66 in MJJAS), TTLCCF ($r = -0.26$ in NDJFM and $r = -0.36$ in MJJAS), ALLCF ($r = -0.26$ in NDJFM and -0.51 in MJJAS), and O₃83 ($r = 0.43$ in NDJFM and $r = 0.72$ in MJJAS). This is despite the stronger QBO–MJO connection and lower-stratospheric temperature impact during boreal winter (Martin et al., 2021; Tegmeier et al., 2020; Yoo & Son, 2016). A seasonality in the QBO’s descent has been well documented (Coy et al., 2020; Dunkerton, 1990). Seasonal changes in the QBO’s explained variance may be a result of a seasonality in the zonal symmetry of the QBO impact on the TTL (Tegmeier et al., 2020). The MJJAS TTL is less variable than that of NDJFM (compare rows 3 and four of Figure S4 in Supporting Information S1), so an equally large QBO signal should be more salient during MJJAS.

The BDC_{EHF} TTL impact maximizes during boreal winter due to increased extratropical stratospheric wave driving (Yulaeva, et al., 1994). NDJFM BDC_{EHF} impacts are larger for CPT, CPZ, and O₃83. The BDC_{EHF} impact on WV83 is comparable during both seasons, but this result is complicated by the strength of the BDC_{EHF} during the two seasons and thus the time of transit between the CPT and 83 hPa (Randel & Park, 2019). WV83 results of Figure 7 are lagged by 1-month (see Section 2.1). Removing this 1-month lag reveals the much stronger BDC_{EHF} control of WV83 during NDJFM compared to MJJAS. We find that the BDC_{EHF} explanation of TTL cirrus clouds is larger during MJJAS (correlation between BDC and TTLCCF is $r = 0.39$ in NDJFM and $r = 0.51$ in MJJAS). This is surprising given the strong connections between the boreal winter BDC_{EHF} and TTL cirrus clouds previously reported (Li & Thompson, 2013), but is not studied further here. Increased explained variance of target variables during NDJFM is partly due to the role of BDC_{PSB}. Although the seasonal cycle in the BDC_{PSB} index has been removed, anomalies are weaker during MJJAS. This may be related to stronger subtropical wave driving variability during NDJFM (Ortland & Alexander, 2014; Randel et al., 2008).

T500’s impact on the target variables is stronger in NDJFM for WV83, TTLCCF, ALLCF, and O₃83. This increase in the tropospheric influence on the TTL variability during these seasons may be related to seasonality in ENSO

activity or tropical wave activity captured by the T500 index (Garfinkel et al., 2018; Orland & Alexander, 2014). The seasonality of the MJO impact on the target variables is more inconsistent and may be further complicated due to aliasing of the Boreal Summer Intraseasonal Oscillation into our MJO index.

4. Discussion and Conclusions

Stratospheric water vapor and TTL cirrus clouds are important components of the climate system but poorly constrained in models. Both exhibit large interannual variability and are linked by temperature in the TTL (Jensen et al., 2013; Tseng & Fu, 2017a). The QBO, BDC_{EHF} , BDC_{PSB} , T500, and MJO contribute to this interannual variability by modulating the dynamic and thermodynamic environment of the TTL (e.g., Davis et al., 2013; Dessler et al., 2013; Randel & Wu, 2015). Multiple linear regressions (MLRs) with modes of the large-scale variability as predictors have been used to study the temperature control of water vapor and TTL cirrus clouds (Austin & Reichler, 2008; Dessler et al., 2014; Garfinkel et al., 2018; Oman et al., 2008). Here we synthesize these results by applying a MLR to CPT, WV83, and TTLCCF and further previous efforts by applying the MLR to ALLCF, CPZ, and O_383 .

The MLR explains significant amounts of variance in CPT (76%), WV83 (65%), TTLCCF (52%), ALLCF (36%), CPZ (78%), and O_383 (62%). Decomposing the explained variance by predictor reveals that for all variables the stratospheric processes explain a larger fraction of the variance. A strong stratospheric predictor of the target variables which received little attention in previous studies is a portion of the shallow branch of the BDC which is not included in BDC_{EHF} but is captured here as BDC_{PSB} . Temperature and BDC_{PSB} correlations have a distinct pattern (see Figure 1p) reminiscent of temperature tendencies caused by subtropical wave driving (Abalos et al., 2014; Grise & Thompson, 2013; Randel et al., 2008). Future work should identify the source of variability of BDC_{PSB} , as it is a significant source of TTL variability. To our knowledge, this is also the first study to show the observed connection between the tropical cold point tropopause temperature and height and global tropospheric and stratospheric temperatures.

Nearly all explained CPT variability comes from the QBO, BDC_{EHF} , and BDC_{PSB} (see Figure 2). Notably, CPT is not correlated with tropical tropospheric temperatures (Figure 3a). In contrast CPZ is controlled by near equal contributions from stratospheric and tropospheric processes. The robust correlation between CPT (CPZ) and stratospheric (stratospheric and tropospheric) temperatures shown in Figure 3a (Figure 4a) can be used to validate model representations of tropopause characteristics. Model simulations suggest that CPZ and CPT increase in response to warming (Austin & Reichler, 2008; Gettelman et al., 2009, 2010; Hardiman et al., 2015; Lin et al., 2017; Wang & Fu, 2023). To the extent that interannual responses to T500 increases can be compared with model simulations of surface warming, observed interannual variability is consistent with model simulations for the CPZ response to tropospheric warming, but not for the CPT response (Lin et al., 2017).

T500 can dynamically induce TTL upwelling. However, T500 can also impact the TTL through thermodynamic processes not directly tied to the upwelling (Bourguet & Linz, 2023; Lin et al., 2017; Ye et al., 2018). To isolate the dynamical impact of T500, the T500 index was separated into the part that was linearly related to the 100 hPa upwelling and that which was not. Our results suggest that the primary influence of T500 on TTLCCF, ALLCF, CPZ and O_383 is via the dynamically induced upwelling (comparing Figures 6 and 2). Notably, the T500 index that is independent of the TTL upwelling is significantly correlated with lower-stratospheric water vapor (Figure 5g) which may be relevant for climate feedbacks (Dessler et al., 2013). While T500 is expected to increase with greenhouse gas concentrations, its interannual variability is greatly influenced by ENSO that is associated with specific SST pattern changes, and thus conclusions relevant to climate change drawn from the results shown here need to be validated by modeling studies.

Because of the CPT's central role in stratospheric water vapor and TTL cloud fraction, it is critically important to understand its interannual variability. The correlation patterns between temperature and residual CPT (after regressing out all modes of variability) still resemble the BDC, with positive (negative) correlations near the tropical (polar) lower stratosphere (Figure 3b). Given that we regressed out both the BDC_{EHF} and BDC_{PSB} indices, this residual CPT correlation resembling the BDC is surprising. Zonal mean temperature data and the CPT timeseries used in Figure 3a comes from RO observations, whereas the BDC_{EHF} and BDC_{PSB} indices come from ERA5, and thus the residual correlation pattern may result from the tropical upwelling quantification from reanalysis. The residual variability in WV83 and O_383 is also correlated with the global stratosphere (Figure S6 in Supporting

Information S1). Future work should thus aim to better understand this dynamical influence of the stratospheric circulation on the CPT.

Data Availability Statement

The data on which this article is based are available in Sweeney and Fu., 2024. Software required to recreate the results is provided in Sweeney (2024).

Acknowledgments

This research is supported by the NASA FINESST Grant 80NSSC22K1438 and NSF Grant AGS-2202812. Additional funding was provided by the Calvin Professorship in Atmospheric Sciences. Part of research was performed when Q.F. visited the University of Cambridge, which was partly supported by the Leverhulme Visiting Professorship. We thank Prof. John M. Wallace, Dr. Mingcheng Wang and Prof. Peter Haynes for their valuable discussions regarding the paper. We also thank the two anonymous reviewers for their help in shaping the scope of the paper, and Dr. Stephen Bourquet for his insight and thoughtful comments which were critical to the final version of the paper.

References

- Abalos, M., Randel, W. J., & Serrano, E. (2012). Variability in upwelling across the tropical tropopause and correlations with tracers in the lower stratosphere. *Atmospheric Chemistry and Physics*, 12(23), 11505–11517. <https://doi.org/10.5194/acp-12-11505-2012>
- Abalos, M., Randel, W. J., & Serrano, E. (2014). Dynamical forcing of subseasonal variability in the tropical Brewer–Dobson circulation. *Journal of the Atmospheric Sciences*, 71(9), 3439–3453. <https://doi.org/10.1175/JAS-D-13-0366.1>
- Anthes, R. A., Bernhardt, P. A., Chen, Y., Cucurull, L., Dymond, K. F., Ector, D., et al. (2008). The COSMIC/FORMOSAT-3 mission: Early results. *Bulletin of the American Meteorological Society*, 89(3), 313–334. <https://doi.org/10.1175/BAMS-89-3-313>
- Austin, J., & Reichler, T. J. (2008). Long-term evolution of the cold point tropical tropopause: Simulation results and attribution analysis. *Journal of Geophysical Research*, 113(D7). <https://doi.org/10.1029/2007JD009768>
- Avery, M. A., Davis, S. M., Rosenlof, K. H., Ye, H., & Dessler, A. E. (2017). Large anomalies in lower stratospheric water vapour and ice during the 2015–2016 El Niño. *Nature Geoscience*, 10(6), 405–409. <https://doi.org/10.1038/ngeo2961>
- Baldwin, M. P., Gray, L. J., Dunkerton, T. J., Hamilton, K., Haynes, P. H., Randel, W. J., et al. (2001). The quasi-biennial oscillation. *Reviews of Geophysics*, 39(2), 179–229. <https://doi.org/10.1029/1999RG000073>
- Banerjee, A., Maycock, A. C., Archibald, A. T., Abraham, N. L., Telford, P., Braesicke, P., & Pyle, J. A. (2016). Drivers of changes in stratospheric and tropospheric ozone between year 2000 and 2100. *Atmospheric Chemistry and Physics*, 16(5), 2727–2746. <https://doi.org/10.5194/acp-16-2727-2016>
- Birner, T., & Charlesworth, E. J. (2017). On the relative importance of radiative and dynamical heating for tropical tropopause temperatures. *Journal of Geophysical Research: Atmospheres*, 122(13), 6782–6797. <https://doi.org/10.1002/2016JD026445>
- Boehm, M. T., & Lee, S. (2003). The implications of tropical rossby waves for tropical tropopause cirrus formation and for the equatorial upwelling of the Brewer–Dobson circulation. *Journal of the Atmospheric Sciences*, 60(2), 247–261. [https://doi.org/10.1175/1520-0469\(2003\)060<0247:TOTRW>2.0.CO;2](https://doi.org/10.1175/1520-0469(2003)060<0247:TOTRW>2.0.CO;2)
- Boehm, M. T., & Verlinde, J. (2000). Stratospheric influence on upper tropospheric tropical cirrus. *Geophysical Research Letters*, 27(19), 3209–3212. <https://doi.org/10.1029/2000GL011678>
- Bourquet, S., & Linz, M. (2023). Weakening of the tropical tropopause layer cold trap with global warming. *Atmospheric Chemistry and Physics*, 23(13), 7447–7460. <https://doi.org/10.5194/acp-23-7447-2023>
- Bramberger, M., Alexander, M. J., Davis, S., Podglajen, A., Hertzog, A., Kalnajs, L., et al. (2022). First super-pressure balloon-borne fine-vertical-scale profiles in the upper TTL: Impacts of atmospheric waves on cirrus clouds and the QBO. *Geophysical Research Letters*, 49(5), e2021GL097596. <https://doi.org/10.1029/2021GL097596>
- Brewer, A. W. (1949). Evidence for a world circulation provided by the measurements of helium and water vapour distribution in the stratosphere. *Quarterly Journal of the Royal Meteorological Society*, 75(326), 351–363. <https://doi.org/10.1002/qj.49707532603>
- Butchart, N., Anstey, J. A., Kawatani, Y., Osprey, S. M., Richter, J. H., & Wu, T. (2020). QBO changes in CMIP6 climate projections. *Geophysical Research Letters*, 47(7), e2019GL086903. <https://doi.org/10.1029/2019GL086903>
- Calvo, N., Garcia, R. R., Randel, W. J., & Marsh, D. R. (2010). Dynamical mechanism for the increase in tropical upwelling in the lowermost tropical stratosphere during warm ENSO events. *Journal of the Atmospheric Sciences*, 67(7), 2331–2340. <https://doi.org/10.1175/2010AS3433.1>
- Chang, K.-W., & L’Ecuyer, T. (2020). Influence of gravity wave temperature anomalies and their vertical gradients on cirrus clouds in the tropical tropopause layer – A satellite-based view. *Atmospheric Chemistry and Physics*, 20(21), 12499–12514. <https://doi.org/10.5194/acp-20-12499-2020>
- Charlesworth, E. J., Birner, T., & Albers, J. R. (2019). Ozone transport-radiation feedbacks in the tropical tropopause layer. *Geophysical Research Letters*, 46(23), 14195–14202. <https://doi.org/10.1029/2019GL084679>
- Chiodo, G., Polvani, L. M., Marsh, D. R., Stenke, A., Ball, W., Rozanov, E., et al. (2018). The response of the ozone layer to Quadrupled CO2 concentrations. *Journal of Climate*, 31(10), 3893–3907. <https://doi.org/10.1175/JCLI-D-17-0492.1>
- Corti, T., Luo, B. P., Fu, Q., Vomel, H., & Peter, T. (2006). The impact of cirrus clouds on tropical troposphere-to-stratosphere transport. *Atmospheric Chemistry and Physics*, 9.
- Coy, L., Newman, P. A., Strahan, S., & Pawson, S. (2020). Seasonal variation of the quasi-biennial oscillation descent. *Journal of Geophysical Research: Atmospheres*, 125(18), e2020JD033077. <https://doi.org/10.1029/2020JD033077>
- Das, S. S., & Suneeth, K. V. (2020). Seasonal and interannual variations of water vapor in the upper troposphere and lower stratosphere over the Asian Summer Monsoon region in perspective of the tropopause and ocean-atmosphere interactions. *Journal of Atmospheric and Solar-Terrestrial Physics*, 201, 105244. <https://doi.org/10.1016/j.jastp.2020.105244>
- Davis, S. M., Liang, C. K., & Rosenlof, K. H. (2013). Interannual variability of tropical tropopause layer clouds. *Geophysical Research Letters*, 40(11), 2862–2866. <https://doi.org/10.1002/grl.50512>
- Deckert, R., & Dameris, M. (2008). Higher tropical SSTs strengthen the tropical upwelling via deep convection. *Geophysical Research Letters*, 35(10). <https://doi.org/10.1029/2008GL033719>
- de Forster, P. M., & Shine, K. P. (1999). Stratospheric water vapour changes as a possible contributor to observed stratospheric cooling. *Geophysical Research Letters*, 26(21), 3309–3312. <https://doi.org/10.1029/1999GL010487>
- Dessler, A. E., Schoeberl, M. R., Wang, T., Davis, S. M., & Rosenlof, K. H. (2013). Stratospheric water vapor feedback. *Proceedings of the National Academy of Sciences*, 110(45), 18087–18091. <https://doi.org/10.1073/pnas.1310344110>
- Dessler, A. E., Schoeberl, M. R., Wang, T., Davis, S. M., Rosenlof, K. H., & Vernier, J.-P. (2014). Variations of stratospheric water vapor over the past three decades. *Journal of Geophysical Research: Atmospheres*, 119(22), 588–598. <https://doi.org/10.1002/2014JD021712>
- Diallo, M., Riese, M., Birner, T., Konopka, P., Müller, R., Hegglin, M. I., et al. (2018). Response of stratospheric water vapor and ozone to the unusual timing of El Niño and the QBO disruption in 2015–2016. *Atmospheric Chemistry and Physics*, 18(17), 13055–13073. <https://doi.org/10.5194/acp-18-13055-2018>

- Ding, Q., & Fu, Q. (2018). A warming tropical central Pacific dries the lower stratosphere. *Climate Dynamics*, *50*(7), 2813–2827. <https://doi.org/10.1007/s00382-017-3774-y>
- Dinh, T. P., Durran, D. R., & Ackerman, T. P. (2010). Maintenance of tropical tropopause layer cirrus. *Journal of Geophysical Research*, *115*(D2). <https://doi.org/10.1029/2009JD012735>
- Dunkerton, T. (1990). Annual variation of deseasonalized mean flow acceleration in the equatorial lower stratosphere. https://doi.org/10.2151/JMSJ1965.68.4_499
- Eguchi, N., & Kodera, K. (2010). Impacts of stratospheric sudden warming event on tropical clouds and moisture fields in the TTL: A case study. *Inside Solaris*, *6*, 137–140. <https://doi.org/10.2151/sola.2010-035>
- Flury, T., Wu, D., & Read, W. (2013). Variability of the Brewer-Dobson circulation's meridional and vertical branch using Aura/MLS water vapor. *Atmospheric Chemistry and Physics Discussions*, *12*, 21291–21320. <https://doi.org/10.5194/acpd-12-21291-2012>
- Flury, T., Wu, D. L., & Read, W. G. (2012). Correlation among cirrus ice content, water vapor and temperature in the TTL as observed by CALIPSO and Aura/MLS. *Atmospheric Chemistry and Physics*, *12*(2), 683–691. <https://doi.org/10.5194/acp-12-683-2012>
- Fu, Q. (2013). Bottom up in the tropics. *Nature Climate Change*, *3*(11), 957–958. <https://doi.org/10.1038/nclimate2039>
- Fu, Q., Hu, Y., & Yang, Q. (2007). Identifying the top of the tropical tropopause layer from vertical mass flux analysis and CALIPSO lidar cloud observations. *Geophysical Research Letters*, *34*(14). <https://doi.org/10.1029/2007GL030099>
- Fu, Q., Lin, P., Solomon, S., & Hartmann, D. L. (2015). Observational evidence of strengthening of the Brewer-Dobson circulation since 1980. *Journal of Geophysical Research: Atmospheres*, *120*(19), 214–228. <https://doi.org/10.1002/2015JD023657>
- Fu, Q., Smith, M., & Yang, Q. (2018). The impact of cloud radiative effects on the tropical tropopause layer temperatures. *Atmosphere*, *9*(10), 377. <https://doi.org/10.3390/atmos9100377>
- Fu, Q., White, R. H., Wang, M., Alexander, B., Solomon, S., Gettelman, A., et al. (2020). The Brewer-Dobson circulation during the last glacial maximum. *Geophysical Research Letters*, *47*(5), e2019GL086271. <https://doi.org/10.1029/2019GL086271>
- Fueglistaler, S., Dessler, A. E., Dunkerton, T. J., Folkins, I., Fu, Q., & Mote, P. W. (2009). Tropical tropopause layer. *Reviews of Geophysics*, *47*(1). <https://doi.org/10.1029/2008RG000267>
- Fueglistaler, S., & Haynes, P. H. (2005). Control of interannual and longer-term variability of stratospheric water vapor. *Journal of Geophysical Research*, *110*(D24). <https://doi.org/10.1029/2005JD006019>
- Garcia, R. R., & Randel, W. J. (2008). Acceleration of the Brewer–Dobson circulation due to increases in greenhouse gases. *Journal of the Atmospheric Sciences*, *65*(8), 2731–2739. <https://doi.org/10.1175/2008JAS2712.1>
- Garfinkel, C. I., Gordon, A., Oman, L. D., Li, F., Davis, S., & Pawson, S. (2018). Nonlinear response of tropical lower stratospheric temperature and water vapor to ENSO. *Atmospheric Chemistry and Physics*, *18*(7), 4597–4615. <https://doi.org/10.5194/acp-18-4597-2018>
- Garfinkel, C. I., Harari, O., Ziskin Ziv, S., Rao, J., Morgenstern, O., Zeng, G., et al. (2021). Influence of the El Niño–Southern Oscillation on entry stratospheric water vapor in coupled chemistry–ocean CCM1 and CMIP6 models. *Atmospheric Chemistry and Physics*, *21*(5), 3725–3740. <https://doi.org/10.5194/acp-21-3725-2021>
- Garfinkel, C. I., & Hartmann, D. L. (2008). Different ENSO teleconnections and their effects on the stratospheric polar vortex. *Journal of Geophysical Research*, *113*(D18). <https://doi.org/10.1029/2008JD009920>
- Garfinkel, C. I., Waugh, D. W., Oman, L. D., Wang, L., & Hurwitz, M. M. (2013). Temperature trends in the tropical upper troposphere and lower stratosphere: Connections with sea surface temperatures and implications for water vapor and ozone. *Journal of Geophysical Research: Atmospheres*, *118*(17), 9658–9672. <https://doi.org/10.1002/jgrd.50772>
- Garny, H., Dameris, M., Randel, W., Bodeker, G. E., & Deckert, R. (2011). Dynamically forced increase of tropical upwelling in the lower stratosphere. *Journal of the Atmospheric Sciences*, *68*(6), 1214–1233. <https://doi.org/10.1175/2011JAS3701.1>
- Gettelman, A., Birner, T., Eyring, V., Akiyoshi, H., Bekki, S., Brühl, C., et al. (2009). The tropical tropopause layer 1960–2100. *Atmospheric Chemistry and Physics*, *9*(5), 1621–1637. <https://doi.org/10.5194/acp-9-1621-2009>
- Gettelman, A., Forster, P. M. F., Fujiwara, M., Fu, Q., Vömel, H., Gohar, L. K., et al. (2004). Radiation balance of the tropical tropopause layer. *Journal of Geophysical Research*, *109*(D7). <https://doi.org/10.1029/2003JD004190>
- Gettelman, A., Hegglin, M. I., Son, S.-W., Kim, J., Fujiwara, M., Birner, T., et al. (2010). Multimodel assessment of the upper troposphere and lower stratosphere: Tropics and global trends. *Journal of Geophysical Research*, *115*(D3). <https://doi.org/10.1029/2009JD013638>
- Grise, K. M., & Thompson, D. W. J. (2013). On the signatures of equatorial and extratropical wave forcing in tropical tropopause layer temperatures. *Journal of the Atmospheric Sciences*, *70*(4), 1084–1102. <https://doi.org/10.1175/JAS-D-12-0163.1>
- Hardiman, S. C., Boutle, I. A., Bushell, A. C., Butchart, N., Cullen, M. J. P., Field, P. R., et al. (2015). Processes controlling tropical tropopause temperature and stratospheric water vapor in climate models. *Journal of Climate*, *28*(16), 6516–6535. <https://doi.org/10.1175/JCLI-D-15-0075.1>
- Haynes, P. H., McIntyre, M. E., Shepherd, T. G., Marks, C. J., & Shine, K. P. (1991). On the “downward control” of extratropical diabatic circulations by eddy-induced mean zonal forces. *Journal of the Atmospheric Sciences*, *48*(4), 651–678. [https://doi.org/10.1175/1520-0469\(1991\)048<0651:OTCOED>2.0.CO;2](https://doi.org/10.1175/1520-0469(1991)048<0651:OTCOED>2.0.CO;2)
- Hersbach, H., Bell, B., Berrisford, P., Hirahara, S., Horányi, A., Muñoz-Sabater, J., et al. (2020). The ERA5 global reanalysis. *Quarterly Journal of the Royal Meteorological Society*, *146*(730), 1999–2049. <https://doi.org/10.1002/qj.3803>
- Holton, J., & Gettelman, A. (2001). Horizontal transport and dehydration in the stratosphere. *Geophysical Research Letters*, *28*(14), 2799–2802. <https://doi.org/10.1029/2001GL013148>
- Holton, J., Haynes, P., McIntyre, M., Douglass, A., Rood, R., & Pfister, L. (1995). Stratosphere-troposphere exchange. *Reviews of Geophysics - REV GEOPHYS*, *33*(4), 403–439. <https://doi.org/10.1029/95RG02097>
- Jensen, E. J., Diskin, G., Lawson, R. P., Lance, S., Bui, T. P., Hlavka, D., et al. (2013). Ice nucleation and dehydration in the tropical tropopause layer. *Proceedings of the National Academy of Sciences*, *110*(6), 2041–2046. <https://doi.org/10.1073/pnas.1217104110>
- Jensen, E. J., Toon, O. B., Pfister, L., & Selkirk, H. B. (1996). Dehydration of the upper troposphere and lower stratosphere by subvisible cirrus clouds near the tropical tropopause. *Geophysical Research Letters*, *23*(8), 825–828. <https://doi.org/10.1029/96GL00722>
- Joshi, M. M., Webb, M. J., Maycock, A. C., & Collins, M. (2010). Stratospheric water vapour and high climate sensitivity in a version of the HadSM3 climate model. *Atmospheric Chemistry and Physics*, *10*(15), 7161–7167. <https://doi.org/10.5194/acp-10-7161-2010>
- Kim, J.-E., & Alexander, M. J. (2015). Direct impacts of waves on tropical cold point tropopause temperature. *Geophysical Research Letters*, *42*(5), 1584–1592. <https://doi.org/10.1002/2014GL062737>
- Kim, J.-E., Alexander, M. J., Bui, T. P., Dean-Day, J. M., Lawson, R. P., Woods, S., et al. (2016). Ubiquitous influence of waves on tropical high cirrus clouds. *Geophysical Research Letters*, *43*(11), 5895–5901. <https://doi.org/10.1002/2016GL069293>
- Kirk-Davidoff, D. B., Hints, E. J., Anderson, J. G., & Keith, D. W. (1999). The effect of climate change on ozone depletion through changes in stratospheric water vapour. *Nature*, *402*(6760), 399–401. <https://doi.org/10.1038/46521>

- Konopka, P., Grooß, J.-U., Plöger, F., & Müller, R. (2009). Annual cycle of horizontal in-mixing into the lower tropical stratosphere. *Journal of Geophysical Research*, *114*(D19). <https://doi.org/10.1029/2009JD011955>
- Konopka, P., Ploeger, F., Tao, M., & Riese, M. (2016). Zonally resolved impact of ENSO on the stratospheric circulation and water vapor entry values. *Journal of Geophysical Research: Atmospheres*, *121*(19), 486–501. <https://doi.org/10.1002/2015JD024698>
- Kuo, Y.-H., Wee, T.-K., Sokolovskiy, S., Rocken, C., Schreiner, W., Hunt, D., & Anthes, R. A. (2004). Inversion and error estimation of GPS radio occultation data. *Journal of the Meteorological Society of Japan. Ser. II*, *82*(1B), 507–531. <https://doi.org/10.2151/jmsj.2004.507>
- Kursinski, E. R., Hajj, G. A., Schofield, J. T., Linfield, R. P., & Hardy, K. R. (1997). Observing Earth's atmosphere with radio occultation measurements using the Global Positioning System. *Journal of Geophysical Research*, *102*(D19), 23429–23465. <https://doi.org/10.1029/97JD01569>
- Li, Y., & Thompson, D. W. J. (2013). The signature of the stratospheric Brewer–Dobson circulation in tropospheric clouds. *Journal of Geophysical Research: Atmospheres*, *118*(9), 3486–3494. <https://doi.org/10.1002/jgrd.50339>
- Liang, C. K., Eldering, A., Gettelman, A., Tian, B., Wong, S., Fetzer, E. J., & Liou, K. N. (2011). Record of tropical interannual variability of temperature and water vapor from a combined AIRS-MLS data set. *Journal of Geophysical Research*, *116*(D6), D06103. <https://doi.org/10.1029/2010JD014841>
- Lin, P., & Fu, Q. (2013). Changes in various branches of the Brewer–Dobson circulation from an ensemble of chemistry climate models. *Journal of Geophysical Research: Atmospheres*, *118*(1), 73–84. <https://doi.org/10.1029/2012JD018813>
- Lin, P., Fu, Q., Solomon, S., & Wallace, J. M. (2009). Temperature trend patterns in southern hemisphere high latitudes: Novel indicators of stratospheric change. *Journal of Climate*, *22*(23), 6325–6341. <https://doi.org/10.1175/2009JCLI2971.1>
- Lin, P., Paynter, D., Ming, Y., & Ramaswamy, V. (2017). Changes of the tropical tropopause layer under global warming. *Journal of Climate*, *30*(4), 1245–1258. <https://doi.org/10.1175/JCLI-D-16-0457.1>
- Lindeman, R. H., Merenda, P. F., & Gold, R. Z. (1980). *Introduction to bivariate and multivariate analysis*. Scott, Foresman.
- Livesey, N. J., Read, W. G., Froidevaux, L., Lambert, A., Santee, M. L., Schwartz, M. J., et al. (2021). Investigation and amelioration of long-term instrumental drifts in water vapor and nitrous oxide measurements from the Aura Microwave Limb Sounder (MLS) and their implications for studies of variability and trends. *Atmospheric Chemistry and Physics*, *21*(20), 15409–15430. <https://doi.org/10.5194/acp-21-15409-2021>
- Lorenz, D. J., & DeWeaver, E. T. (2007). Tropopause height and zonal wind response to global warming in the IPCC scenario integrations. *Journal of Geophysical Research*, *112*(D10). <https://doi.org/10.1029/2006JD008087>
- Lu, J., Xie, F., Sun, C., Luo, J., Cai, Q., Zhang, J., et al. (2020). Analysis of factors influencing tropical lower stratospheric water vapor during 1980–2017. *Npj Climate and Atmospheric Science*, *3*(1), 1–11. <https://doi.org/10.1038/s41612-020-00138-7>
- Madden, R. A., & Julian, P. R. (1971). Detection of a 40–50 Day oscillation in the zonal wind in the tropical pacific. *Journal of the Atmospheric Sciences*, *28*(5), 702–708. [https://doi.org/10.1175/1520-0469\(1971\)028<0702:DOADOI>2.0.CO;2](https://doi.org/10.1175/1520-0469(1971)028<0702:DOADOI>2.0.CO;2)
- Marsh, D. R., & Garcia, R. R. (2007). Attribution of decadal variability in lower-stratospheric tropical ozone. *Geophysical Research Letters*, *34*(21). <https://doi.org/10.1029/2007GL030935>
- Martin, Z., Sobel, A., Butler, A., & Wang, S. (2021). Variability in QBO temperature anomalies on annual and decadal time scales. *Journal of Climate*, *34*(2), 589–605. <https://doi.org/10.1175/JCLI-D-20-0287.1>
- Match, A., & Gerber, E. P. (2022). Tropospheric expansion under global warming reduces tropical lower stratospheric ozone. *Geophysical Research Letters*, *49*(19), e2022GL099463. <https://doi.org/10.1029/2022GL099463>
- McFarquhar, G. M., Heymsfield, A. J., Spinhirne, J., & Hart, B. (2000). Thin and subvisual tropopause tropical cirrus: Observations and radiative impacts. *Journal of the Atmospheric Sciences*, *57*(12), 1841–1853. [https://doi.org/10.1175/1520-0469\(2000\)057<1841:TASTTC>2.0.CO;2](https://doi.org/10.1175/1520-0469(2000)057<1841:TASTTC>2.0.CO;2)
- Mote, P. W., Rosenlof, K. H., McIntyre, M. E., Carr, E. S., Gille, J. C., Holton, J. R., et al. (1996). An atmospheric tape recorder: The imprint of tropical tropopause temperatures on stratospheric water vapor. *Journal of Geophysical Research*, *101*(D2), 3989–4006. <https://doi.org/10.1029/95JD03422>
- Oman, L., Waugh, D. W., Pawson, S., Stolarski, R. S., & Nielsen, J. E. (2008). Understanding the changes of stratospheric water vapor in coupled chemistry–climate model simulations. *Journal of the Atmospheric Sciences*, *65*(10), 3278–3291. <https://doi.org/10.1175/2008JAS2696.1>
- Ortlund, D. A., & Alexander, M. J. (2014). The residual-mean circulation in the tropical tropopause layer driven by tropical waves. *Journal of the Atmospheric Sciences*, *71*(4), 1305–1322. <https://doi.org/10.1175/JAS-D-13-0100.1>
- Pahlavan, H. A., Fu, Q., Wallace, J. M., & Kiladis, G. N. (2021). Revisiting the quasi-biennial oscillation as seen in ERA5. Part I: Description and momentum budget. *Journal of the Atmospheric Sciences*, *78*(3), 673–691. <https://doi.org/10.1175/JAS-D-20-0248.1>
- Philander, G. (1990). *Geophysical Interplays: El Niño, La Niña, and the Southern Oscillation*. S. George Philander. Academic Press, San Diego, CA, 1989. x, 293 pp., illus. \$59.50. International Geophysics Series, vol. 46. *Science*, *248*(4957), 904–905. <https://doi.org/10.1126/science.248.4957.904>
- Plumb, R. A., & Bell, R. C. (1982). Equatorial waves in steady zonal shear flow. *Quarterly Journal of the Royal Meteorological Society*, *108*(456), 313–334. <https://doi.org/10.1002/qj.49710845603>
- Plumb, R. A., & Eluszkiewicz, J. (1999). The Brewer–Dobson Circulation: Dynamics of the Tropical Upwelling. *Journal of the Atmospheric Sciences*, *56*(6), 868–890. [https://doi.org/10.1175/1520-0469\(1999\)056<0868:TBDCDO>2.0.CO;2](https://doi.org/10.1175/1520-0469(1999)056<0868:TBDCDO>2.0.CO;2)
- Podglajen, A., Hertzog, A., Plougonven, R., & Legras, B. (2016). Lagrangian temperature and vertical velocity fluctuations due to gravity waves in the lower stratosphere. *Geophysical Research Letters*, *43*(7), 3543–3553. <https://doi.org/10.1002/2016GL068148>
- Podglajen, A., Plougonven, R., Hertzog, A., & Jensen, E. (2018). Impact of gravity waves on the motion and distribution of atmospheric ice particles. *Atmospheric Chemistry and Physics*, *18*(14), 10799–10823. <https://doi.org/10.5194/acp-18-10799-2018>
- Randel, W., & Park, M. (2019). Diagnosing Observed Stratospheric Water Vapor Relationships to the Cold Point Tropical Tropopause. *Journal of Geophysical Research: Atmospheres*, *124*(13), 7018–7033. <https://doi.org/10.1029/2019JD030648>
- Randel, W. J., Garcia, R., & Wu, F. (2008). Dynamical Balances and Tropical Stratospheric Upwelling. *Journal of the Atmospheric Sciences*, *65*(11), 3584–3595. <https://doi.org/10.1175/2008JAS2756.1>
- Randel, W. J., Garcia, R. R., Calvo, N., & Marsh, D. (2009). ENSO influence on zonal mean temperature and ozone in the tropical lower stratosphere. *Geophysical Research Letters*, *36*(15). <https://doi.org/10.1029/2009GL039343>
- Randel, W. J., Garcia, R. R., & Wu, F. (2002). Time-Dependent Upwelling in the Tropical Lower Stratosphere Estimated from the Zonal-Mean Momentum Budget. *Journal of the Atmospheric Sciences*, *59*(13), 2141–2152. [https://doi.org/10.1175/1520-0469\(2002\)059<2141:TDUITT>2.0.CO;2](https://doi.org/10.1175/1520-0469(2002)059<2141:TDUITT>2.0.CO;2)
- Randel, W. J., & Jensen, E. J. (2013). Physical processes in the tropical tropopause layer and their roles in a changing climate. *Nature Geoscience*, *6*(3), 169–176. <https://doi.org/10.1038/ngeo1733>
- Randel, W. J., Park, M., Emmons, L., Kinnison, D., Bernath, P., Walker, K. A., et al. (2010). Asian Monsoon Transport of Pollution to the Stratosphere. *Science*, *328*(5978), 611–613. <https://doi.org/10.1126/science.1182274>
- Randel, W. J., Park, M., Wu, F., & Livesey, N. (2007). A Large Annual Cycle in Ozone above the Tropical Tropopause Linked to the Brewer–Dobson Circulation. *Journal of the Atmospheric Sciences*, *64*(12), 4479–4488. <https://doi.org/10.1175/2007JAS2409.1>

- Randel, W. J., & Wu, F. (2015). Variability of Zonal Mean Tropical Temperatures Derived from a Decade of GPS Radio Occultation Data. *Journal of the Atmospheric Sciences*, 72(3), 1261–1275. <https://doi.org/10.1175/JAS-D-14-0216.1>
- Randel, W. J., Wu, F., & Gaffen, D. J. (2000). Interannual variability of the tropical tropopause derived from radiosonde data and NCEP reanalyses. *Journal of Geophysical Research*, 105(D12), 15509–15523. <https://doi.org/10.1029/2000JD900155>
- Read, W. G., Lambert, A., Bacmeister, J., Cofield, R. E., Christensen, L. E., Cuddy, D. T., et al. (2007). Aura Microwave Limb Sounder upper tropospheric and lower stratospheric H₂O and relative humidity with respect to ice validation. *Journal of Geophysical Research (Atmospheres)*, 112(D24), D24S35. <https://doi.org/10.1029/2007JD008752>
- Richter, J. H., Anstey, J. A., Butchart, N., Kawatani, Y., Meehl, G. A., Osprey, S., & Simpson, I. R. (2020). Progress in Simulating the Quasi-Biennial Oscillation in CMIP Models. *Journal of Geophysical Research: Atmospheres*, 125(8), e2019JD032362. <https://doi.org/10.1029/2019JD032362>
- Rosenlof, K. H. (1995). Seasonal cycle of the residual mean meridional circulation in the stratosphere. *Journal of Geophysical Research*, 100(D3), 5173–5191. <https://doi.org/10.1029/94JD03122>
- Santee, M. L., Manney, G. L., Livesey, N. J., Schwartz, M. J., Neu, J. L., & Read, W. G. (2017). A comprehensive overview of the climatological composition of the Asian summer monsoon anticyclone based on 10 years of Aura Microwave Limb Sounder measurements. *Journal of Geophysical Research: Atmospheres*, 122(10), 5491–5514. <https://doi.org/10.1002/2016JD026408>
- Santer, B. D., Sausen, R., Wigley, T. M. L., Boyle, J. S., AchutaRao, K., Doutriaux, C., et al. (2003). Behavior of tropopause height and atmospheric temperature in models, reanalyses, and observations: Decadal changes. *Journal of Geophysical Research*, 108(D1). ACL 1-1-ACL 1-22. <https://doi.org/10.1029/2002JD002258>
- Scherlin-Pirscher, B., Deser, C., Ho, S.-P., Chou, C., Randel, W., & Kuo, Y.-H. (2012). The vertical and spatial structure of ENSO in the upper troposphere and lower stratosphere from GPS radio occultation measurements. *Geophysical Research Letters*, 39(20). <https://doi.org/10.1029/2012GL053071>
- Schreiner, W. S., Weiss, J. P., Anthes, R. A., Braun, J., Chu, V., Fong, J., et al. (2020). COSMIC-2 Radio Occultation Constellation: First Results. *Geophysical Research Letters*, 47(4), e2019GL086841. <https://doi.org/10.1029/2019GL086841>
- Shepherd, T. G., & McLandress, C. (2011). A Robust Mechanism for Strengthening of the Brewer–Dobson Circulation in Response to Climate Change: Critical-Layer Control of Subtropical Wave Breaking. *Journal of the Atmospheric Sciences*, 68(4), 784–797. <https://doi.org/10.1175/2010JAS3608.1>
- Sokol, A. B., & Hartmann, D. L. (2020). Tropical Anvil Clouds: Radiative Driving Toward a Preferred State. *Journal of Geophysical Research: Atmospheres*, 125(21), e2020JD033107. <https://doi.org/10.1029/2020JD033107>
- Solomon, S., Ivy, D. J., Kinnison, D., Mills, M. J., Neely, R. R., & Schmidt, A. (2016). Emergence of healing in the Antarctic ozone layer. *Science*, 353(6296), 269–274. <https://doi.org/10.1126/science.aae0061>
- Solomon, S., Rosenlof, K. H., Portmann, R. W., Daniel, J. S., Davis, S. M., Sanford, T. J., & Plattner, G.-K. (2010). Contributions of Stratospheric Water Vapor to Decadal Changes in the Rate of Global Warming. *Science*, 327(5970), 1219–1223. <https://doi.org/10.1126/science.1182488>
- Sunilkumar, S. V., Parameswaran, K., Rajeev, K., Krishna Murthy, B. V., Meenu, S., Mehta, S. K., & Babu, A. (2010). Semitransparent cirrus clouds in the tropical tropopause layer during two contrasting seasons. *Journal of Atmospheric and Solar-Terrestrial Physics*, 72(9), 745–762. <https://doi.org/10.1016/j.jastp.2010.03.020>
- Sweeney, A. (2024). Release Version (1.0.0) AodhanSweeney/TTLVariability. [Software]. Zenodo, <https://doi.org/10.5281/zenodo.10465407>
- Sweeney, A., & Fu, Q. (2024). Interannual Variability of Zonal Mean Temperature, Water Vapor, and Clouds in the Tropical Tropopause Layer. [Dataset]. Zenodo, <https://doi.org/10.5281/zenodo.10463640>
- Sweeney, A., Fu, Q., Pahlavan, H. A., & Haynes, P. (2023). Seasonality of the QBO Impact on Equatorial Clouds. *Journal of Geophysical Research: Atmospheres*, 128(7), e2022JD037737. <https://doi.org/10.1029/2022JD037737>
- Sweeney, A. J., & Fu, Q. (2021). Diurnal Cycles of Synthetic Microwave Sounding Lower-Stratospheric Temperatures from Radio Occultation Observations, Reanalysis, and Model Simulations. *Journal of Atmospheric and Oceanic Technology*, 38(12), 2045–2059. <https://doi.org/10.1175/JTECH-D-21-0071.1>
- Tegtmeier, S., Anstey, J., Davis, S., Ivanciu, I., Jia, Y., McPhee, D., & Pilch Kedzierski, R. (2020). Zonal Asymmetry of the QBO Temperature Signal in the Tropical Tropopause Region. *Geophysical Research Letters*, 47(24), e2020GL089533. <https://doi.org/10.1029/2020GL089533>
- Thornberry, T. D., Rollins, A. W., Avery, M. A., Woods, S., Lawson, R. P., Bui, T. V., & Gao, R.-S. (2017). Ice water content-extinction relationships and effective diameter for TTL cirrus derived from in situ measurements during ATTREX 2014. *Journal of Geophysical Research: Atmospheres*, 122(8), 4494–4507. <https://doi.org/10.1002/2016JD025948>
- Thorsen, T. J., Fu, Q., Comstock, J. M., Sivaraman, C., Vaughan, M. A., Winker, D. M., & Turner, D. D. (2013). Macrophysical properties of tropical cirrus clouds from the CALIPSO satellite and from ground-based micropulse and Raman lidars. *Journal of Geophysical Research: Atmospheres*, 118(16), 9209–9220. <https://doi.org/10.1002/jgrd.50691>
- Tian, E. W., Su, H., Tian, B., & Jiang, J. H. (2019). Interannual variations of water vapor in the tropical upper troposphere and the lower and middle stratosphere and their connections to ENSO and QBO. *Atmospheric Chemistry and Physics*, 19(15), 9913–9926. <https://doi.org/10.5194/acp-19-9913-2019>
- Tseng, H.-H., & Fu, Q. (2017a). Tropical tropopause layer cirrus and its relation to tropopause. *Journal of Quantitative Spectroscopy and Radiative Transfer*, 188, 118–131. <https://doi.org/10.1016/j.jqsrt.2016.05.029>
- Tseng, H.-H., & Fu, Q. (2017b). Temperature Control of the Variability of Tropical Tropopause Layer Cirrus Clouds. *Journal of Geophysical Research: Atmospheres*, 122(20), 062–075. <https://doi.org/10.1002/2017JD027093>
- Tweedy, O. V., Waugh, D. W., Randel, W. J., Abalos, M., Oman, L. D., & Kinnison, D. E. (2018). The Impact of Boreal Summer ENSO Events on Tropical Lower Stratospheric Ozone. *Journal of Geophysical Research: Atmospheres*, 123(17), 9843–9857. <https://doi.org/10.1029/2018JD029020>
- Ueyama, R., Jensen, E. J., & Pfister, L. (2018). Convective Influence on the Humidity and Clouds in the Tropical Tropopause Layer During Boreal Summer. *Journal of Geophysical Research: Atmospheres*, 123(14), 7576–7593. <https://doi.org/10.1029/2018JD028674>
- Ueyama, R., Jensen, E. J., Pfister, L., & Kim, J.-E. (2015). Dynamical, convective, and microphysical control on wintertime distributions of water vapor and clouds in the tropical tropopause layer. *Journal of Geophysical Research: Atmospheres*, 120(19), 483–500. <https://doi.org/10.1002/2015JD023318>
- Ventrice, M., Wheeler, M., Hendon, H., Iii, S., Thorncroft, C., & Kiladis, G. (2013). A Modified Multivariate Madden-Julian Oscillation Index Using Velocity Potential. *Monthly Weather Review*, 141(12), 4197–4210. <https://doi.org/10.1175/MWR-D-12-00327.1>
- Virts, K. S., & Wallace, J. M. (2014). Observations of Temperature, Wind, Cirrus, and Trace Gases in the Tropical Tropopause Transition Layer during the MJO. *Journal of the Atmospheric Sciences*, 71(3), 1143–1157. <https://doi.org/10.1175/JAS-D-13-0178.1>
- Virts, K. S., Wallace, J. M., Fu, Q., & Ackerman, T. P. (2010). Tropical Tropopause Transition Layer Cirrus as Represented by CALIPSO Lidar Observations. *Journal of the Atmospheric Sciences*, 67(10), 3113–3129. <https://doi.org/10.1175/2010JAS3412.1>

- Walker, J. M., Bordoni, S., & Schneider, T. (2015). Interannual Variability in the Large-Scale Dynamics of the South Asian Summer Monsoon. *Journal of Climate*, 28(9), 3731–3750. <https://doi.org/10.1175/JCLI-D-14-00612.1>
- Wang, M., & Fu, Q. (2021). Stratosphere-Troposphere Exchange of Air Masses and Ozone Concentrations Based on Reanalyses and Observations. *Journal of Geophysical Research: Atmospheres*, 126(18), e2021JD035159. <https://doi.org/10.1029/2021JD035159>
- Wang, M., & Fu, Q. (2023). Changes in Stratosphere-Troposphere Exchange of Air Mass and Ozone Concentration in CCM1 Models From 1960 to 2099. *Journal of Geophysical Research: Atmospheres*, 128(13), e2023JD038487. <https://doi.org/10.1029/2023JD038487>
- Wang, T., Wu, D. L., Gong, J., & Tsai, V. (2019). Tropopause Laminar Cirrus and Its Role in the Lower Stratosphere Total Water Budget. *Journal of Geophysical Research: Atmospheres*, 124(13), 7034–7052. <https://doi.org/10.1029/2018JD029845>
- Winker, D. M., Pelon, J., Coakley, J. A., Ackerman, S. A., Charlson, R. J., Colarco, P. R., et al. (2010). The CALIPSO Mission: A Global 3D View of Aerosols and Clouds. *Bulletin of the American Meteorological Society*, 91(9), 1211–1230. <https://doi.org/10.1175/2010BAMS3009.1>
- Wu, Y., & Zheng, C. (2022). Summertime Transport Pathways and Dynamics From Northern India and Tibetan Plateau to the Lower Stratosphere: Insights From Idealized Tracer Experiments. *Journal of Geophysical Research: Atmospheres*, 127(9), e2021JD036399. <https://doi.org/10.1029/2021JD036399>
- Xie, F., Li, J., Tian, W., Li, Y., & Feng, J. (2014). Indo-Pacific Warm Pool Area Expansion, Modoki Activity and Tropical Cold-Point Tropopause Temperature Variations. *Scientific Reports*, 4(1), 4552. <https://doi.org/10.1038/srep04552>
- Yang, Q., Fu, Q., & Hu, Y. (2010). Radiative impacts of clouds in the tropical tropopause layer. *Journal of Geophysical Research*, 115(D4). <https://doi.org/10.1029/2009JD012393>
- Ye, H., Dessler, A. E., & Yu, W. (2018). Effects of convective ice evaporation on interannual variability of tropical tropopause layer water vapor. *Atmospheric Chemistry and Physics*, 18(7), 4425–4437. <https://doi.org/10.5194/acp-18-4425-2018>
- Yoo, C., & Son, S.-W. (2016). Modulation of the boreal wintertime Madden-Julian oscillation by the stratospheric quasi-biennial oscillation. *Geophysical Research Letters*, 43(3), 1392–1398. <https://doi.org/10.1002/2016GL067762>
- Yulaeva, E., Holton, J. R., & Wallace, J. M. (1994). On the Cause of the Annual Cycle in Tropical Lower-Stratospheric Temperatures. *Journal of the Atmospheric Sciences*, 51(2), 169–174. [https://doi.org/10.1175/1520-0469\(1994\)051<0169:OTCOTA>2.0.CO;2](https://doi.org/10.1175/1520-0469(1994)051<0169:OTCOTA>2.0.CO;2)
- Zeng, Z., Sokolovskiy, S., Schreiner, W. S., & Hunt, D. (2019). Representation of Vertical Atmospheric Structures by Radio Occultation Observations in the Upper Troposphere and Lower Stratosphere: Comparison to High-Resolution Radiosonde Profiles. *Journal of Atmospheric and Oceanic Technology*, 36(4), 655–670. <https://doi.org/10.1175/JTECH-D-18-0105.1>
- Zhou, C., Dessler, A. E., Zelinka, M. D., Yang, P., & Wang, T. (2014). Cirrus feedback on interannual climate fluctuations. *Geophysical Research Letters*, 41(24), 9166–9173. <https://doi.org/10.1002/2014GL062095>
- Ziskin Ziv, S., Garfinkel, C. I., Davis, S., & Banerjee, A. (2022). The roles of the Quasi-Biennial Oscillation and El Niño for entry stratospheric water vapor in observations and coupled chemistry–ocean CCM1 and CMIP6 models. *Atmospheric Chemistry and Physics*, 22(11), 7523–7538. <https://doi.org/10.5194/acp-22-7523-2022>